

A group-theoretic approach to the origin of chirality-induced spin selectivity in non-magnetic molecular junctions

W. Dednam^{1,*}, M. A. García-Blázquez^{2,*}, Linda A. Zotti^{3,4}, E. B. Lombardi¹, C. Sabater⁵, S. Pakdel⁶, and J. J. Palacios^{2,7} ✉

¹ Department of Physics, Florida Science Campus, University of South Africa, 1710 Johannesburg, South Africa

² Departamento de Física de la Materia Condensada, Universidad Autónoma de Madrid, E-28049 Madrid, Spain

³ Departamento de Física Teórica de la Materia Condensada, Universidad Autónoma de Madrid, E-28049 Madrid, Spain

⁴ Condensed Matter Physics Center (IFIMAC), Universidad Autónoma de Madrid, E-28049 Madrid, Spain

⁵ Departamento de Física Aplicada and Unidad asociada CSIC, Universidad de Alicante, E-03690 Alicante, Spain

⁶ CAMD, Department of Physics, Technical University of Denmark, 2800 Kgs. Lyngby, Denmark

⁷ Instituto Nicolás Cabrera (INC) and Condensed Matter Physics Center (IFIMAC), Universidad Autónoma de Madrid, E-28049 Madrid, Spain

* These authors contributed equally to this work

✉ e-mail: juanjose.palacios@uam.es

ABSTRACT

Spin-orbit coupling gives rise to a range of spin-charge interconversion phenomena in non-magnetic systems where spatial symmetries are reduced or absent. Chirality-induced spin selectivity (CISS), a term that generically refers to a spin-dependent electron transfer in non-magnetic chiral systems, is one such case, appearing in a variety of seemingly unrelated situations ranging from inorganic materials to molecular devices. In particular, the origin of CISS in molecular junctions is a matter of an intense current debate. Here we contend that the necessary conditions for the CISS effect to appear can be generally and fully understood on the basis of a complete symmetry analysis of the molecular junction, and not only of the molecule. Our approach, which draws on the use of point-group symmetries within the scattering formalism for transport, shows that electrode symmetries are as important as those of the molecule when it comes to the emergence of a spin-polarization and, therefore, a possible appearance of CISS. It turns out that standalone metallic nanocontacts can exhibit spin-polarization when relative rotations are introduced which reduce the symmetry. As a corollary, molecular junctions with *achiral* molecules can also exhibit spin polarization along the direction of transport, provided that the whole junction is chiral. This formalism also allows to predict the qualitative changes on the spin-polarization upon substitution of a chiral molecule in the junction with its enantiomeric partner. Quantum transport calculations based on density functional theory corroborate all of our predictions and provide further quantitative insight.

Taking advantage of the spin degree of freedom in non-magnetic materials relies on our ability to leverage the combination of strong spin-orbit coupling (SOC) and structural asymmetries. Prototypical examples where this combination occurs include free surfaces of heavy metals^{1,2} and topological insulators³, two-dimensional (2D) electron gases⁴, semiconductor thin films⁵, or 2D crystals with intentionally broken mirror symmetry⁶⁻⁹. More recently, chiral bulk systems such as Te crystals, where inversion and mirror symmetries are absent, are also being explored¹⁰. In all these systems spin-related phenomena such as the spin Hall¹¹⁻¹³ or Edelstein¹⁴ effects (both inverse and direct) can appear and serve as a basis for exploiting the full potential of spin for spintronics applications. On the theoretical side, from basic 2D electron gas models¹⁵⁻¹⁷ to more sophisticated models based on first-principles^{7,18,19}, many of the experimental observations can be successfully accounted for.

Molecular junctions with chiral molecules are also a playground for spin-charge interconversion phenomena, exhibiting the so-called chirality-induced spin selectivity (CISS) effect. This phenomenon, which is essentially analogous to the Edelstein effect in crystals, has been the subject of a large number of experimental²⁰⁻³¹ and theoretical studies³²⁻⁴⁶ over the past few years. The CISS effect in this context is usually identified with a finite magneto-conductance measured in transport experiments in the non-linear response regime^{37,38,47}. The microscopic origin of the CISS effect is being actively debated and may be attributed to a combination of factors such as the chirality of the molecule, the strength of SOC in the system, electron correlations, dephasing effects, and a finite bias voltage^{43,47-53}. At least one of these factors, the strength of SOC in the normal metal

electrode component of the junction, has been unambiguously identified as driving large a magneto-conductance in molecular junctions^{27,30}. A strong SOC in combination with the chirality of the molecules facilitate the appearance of a significant spin-polarization (or spin current), which appears to be a necessary condition for the CISS effect to ultimately manifest in experiments. Given that chirality, a symmetry property of the system, is at the core of the terminology itself, it seems particularly appropriate to employ group theory to analyze the emergence of spin-polarization, yet a complete and rigorous treatment appears to be missing in the literature.

In this work we present a systematic and complete theoretical analysis of the electronic spin-polarization in molecular junctions (non-magnetic CISS devices), based entirely on the use of the point symmetry group of the whole system (electrodes plus, possibly, a molecule) within the scattering formulation of quantum transport. This analysis allows us to determine the restrictions imposed by each individual spatial symmetry on the relevant quantities of the problem, the spin-resolved conductance and the spin-polarization. We list the possible symmetries that can be found in the two-terminal configurations and identify those which, when removed, allow for polarization to appear in the general case –regardless of the system being a standalone pair of metallic nanocontacts, or a molecular junction with a chiral or achiral molecule. In particular, we show that a simple relative rotation of the electrodes, leading to the removal of certain mirror symmetries, is in general sufficient for the spin-polarization to emerge, independently of the chiral nature of the molecule or even its sheer presence.

At a quantitative level we present density functional theory (DFT) calculations for realistic systems which corroborate and quantify our theoretical predictions. We find a significant spin-polarization for organic molecules as long as the electrodes, not necessarily the molecule, present a strong SOC, specific mirror symmetries are removed and the orbital character near the Fermi level is not exclusively s -type. Chiral molecules, as expected, give rise to spin-polarization in general. Naively one may expect that the substitution of a chiral molecule by its enantiomeric partner in a molecular junction would result in the exact reversal of the spin-polarization. However, we show that this phenomenon is more subtle, requiring certain geometrical conditions on the electrodes as well as on the specific anchoring of the molecules for spin-polarization to be strictly reversed. In summary, our results grant a rather general view of the origin of the spin-polarization in transport in molecular junctions with non-magnetic electrodes, constituting a global framework with which one can predict the necessary (not sufficient) conditions under which the CISS effect can be observed.

Symmetry considerations

We consider a two-terminal device formed by two electrodes or contacts and, possibly, a molecule between them. The component along the direction of an arbitrary spin quantization axis of the spin-polarization of the current generated at the drain electrode is, for an incident unpolarized current¹⁶:

$$P = G_{\uparrow\uparrow} + G_{\uparrow\downarrow} - G_{\downarrow\uparrow} - G_{\downarrow\downarrow} \quad (1)$$

where $G_{s',s}$ ($s, s' \in \{\uparrow, \downarrow\}$ referred to the spin axis) is the spin-resolved conductance at a given energy (which we omit for simplicity) measured relative to the Fermi energy. The three components of the vector \mathbf{P} can then be obtained by rotating the quantization axis and applying (1).

As a position-independent quantity which in the scattering formalism can be computed, at least formally, from the electronic wave functions of the electrodes and the Hamiltonian of the system, $G_{s',s}$ may in principle be subject to restrictions induced by the spatial symmetries of the whole system. These relations are obtained by recalling the invariance of the corresponding space integrals under the orthogonal coordinate transformations which form the point group \mathcal{G} of the system (electrodes plus, possibly, molecule) and employing the (projective) representations according to which the spinor wave functions in the electrodes transform. The complete derivation can be found in *Methods*, from which it follows that only symmetries which do not permute the electrodes can potentially impose a restriction (5) on the original conductance. In contrast, symmetries which do permute the electrodes may only yield a relation (6) between the original conductance and that corresponding to the hypothetical situation where bias polarity is reversed. The latter assertion also applies to anti-unitary symmetries, i.e., time-reversal and potentially particle-hole, which can be freely applied within the scalar products up to complex conjugation.

Specifically, from equation (5) it follows that a relation between the spin-resolved conductance terms $G_{s',s}$ may arise only if the junction presents the following spatial symmetries:

- A $2\pi/n$ -rotation C_n which does not permute the electrodes. For a spin quantization axis directed along rotation axis, the condition on the conductance is trivial; however, for $n = 2$ and any quantization axis perpendicular to the rotation axis, $G_{s',s} = G_{\bar{s}',\bar{s}}$ where \bar{s} corresponds to the opposite spin state of s . Hence, by (1) the components of the spin-polarization which are normal to the rotation axis vanish. In our collinear two-terminal configuration, this rotation axis must coincide with the longitudinal direction (along which transport takes place) and we denote the operation by $C_{n,l}$.
- A mirror plane σ which does not permute the electrodes. Since the spinors transform as pseudo-vectors, in our formalism this operation is essentially equivalent (except for the invariance of the electrodes) to a π -rotation about the axis which

Table 1. Conditions imposed on the spin resolved conductance terms (2) and the resulting spin-polarization vector \mathbf{P} by the spatial symmetries of the whole system (electrodes with possibly a molecule between them) on their own, as well as in combination with time reversal symmetry Θ . Columns: **1**, Element of the point group \mathcal{G} of the system. **2**, Direction of spin projection, which defines the polarization component (1). **3**, Conductance term to which $G_{s',\bar{s}}^{AB}$ must be equal, due to the presence of either **3.1**, the spatial symmetry alone (5), (6), or **3.2**, the spatial symmetry together with time reversal (7), (8). \bar{s} corresponds to the opposite spin state of s , and G^{BA} to the conductance from electrode B to electrode A . **4**, Restriction imposed on the corresponding vector components of the spin-polarization. Entries in blank are either tautological or inconclusive (yield no compact identities). Anti-unitary symmetries have been included in the last two rows.

Symmetry ($g \in \mathcal{G}$)	Spin quantization axis	$G_{s',\bar{s}}^{AB}$ identity		\mathbf{P} restriction
		g	Θg	
Longitudinal mirror (σ_l)	Longitudinal (l)	$G_{s',\bar{s}}^{AB}$	$G_{s,s'}^{BA}$	$P_l = 0$
	Transversal, parallel to σ_l (t_{\parallel})	$G_{s',\bar{s}}^{AB}$	$G_{s,s'}^{BA}$	$P_{t_{\parallel}} = 0$
	Transversal, normal to σ_l (t_{\perp})			
Longitudinal π -rotation ($C_{2,l}$)	Longitudinal (l)			
	Transversal (t)	$G_{s',\bar{s}}^{AB}$	$G_{s,s'}^{BA}$	$P_t = 0$
Longitudinal $2\pi/n$ -rotation ($C_{n,l}$), $n \geq 3$	Longitudinal (l)			
	Transversal (t)			$P_t = 0$
Transversal mirror (σ_t)	Longitudinal (l)	$G_{s',s}^{BA}$	$G_{\bar{s},s'}^{AB}$	
	Transversal (t)	$G_{s',\bar{s}}^{BA}$	$G_{s,s'}^{AB}$	
Transversal π -rotation ($C_{2,t}$)	Longitudinal (l)	$G_{s',\bar{s}}^{BA}$	$G_{s,s'}^{AB}$	
	Transversal, parallel to $C_{2,t}$ (t_{\parallel})	$G_{s',s}^{BA}$	$G_{\bar{s},s'}^{AB}$	
	Transversal, normal to $C_{2,t}$ (t_{\perp})	$G_{s',\bar{s}}^{BA}$	$G_{s,s'}^{AB}$	
Inversion (I_s)	Any	$G_{s',s}^{BA}$	$G_{\bar{s},s'}^{AB}$	
Time-reversal (Θ)	Any	$G_{s,\bar{s}'}^{BA}$		$\mathbf{P} = 0$ if 1 channel at B
Particle-hole (\mathcal{C})	Any	$G_{s,s'}^{BA}(-E)$	$G_{s',\bar{s}}^{AB}(-E)$	$\mathbf{P}(E) = -\mathbf{P}(-E)$

is perpendicular to the mirror plane and contains the fixed point of \mathcal{G} . By the previous case, the components of the spin-polarization \mathbf{P} which are parallel to the mirror plane must vanish. In our configuration, this plane must contain the longitudinal direction, and we denote the operation by σ_l (note, however, that there will in general be more than one longitudinal plane of symmetry). We refer to any direction perpendicular to the longitudinal one as transversal, in particular the direction in which \mathbf{P} points (unless it is the zero vector) in this case.

A careful analysis reveals one further restriction (12) on the polarization which is not associated with identities between the different conductance terms: *any longitudinal rotation symmetry $C_{n,l}$ ($n \geq 2$), not only $C_{2,l}$, guarantees the vanishing of all the transversal components of the spin-polarization*. Only rotations with $n = 2, 3, 4, 6$ are, however, allowed in electrodes which possess a three-dimensional crystalline structure in the bulk. In contrast, chain-like electrodes may present other $C_{n,l}$

symmetries, with one-atom chains presenting any of them.

We thus conclude that *there can be no spin-polarization in two-terminal systems whose point group \mathcal{G} is one of the following: C_{nv} , D_{nh} , D_{nd} , $\forall n \geq 2$* , (where the principal rotation axis is oriented along the longitudinal direction) due to the simultaneous presence of $C_{n,l}$ and σ_l , which forces all the vector components of the spin-polarization to vanish. Note that the polyhedral groups are not compatible with a two-terminal configuration, hence are automatically excluded. Several examples are shown in Fig. 1 and discussed in the next section. The remaining groups which may admit a finite polarization vector, C_i , $C_{2n,h}$, S_{4n-2} , $\forall n \geq 1$, contain inversion symmetry, the geometrical breaking of which is thus not a necessary condition to observe spin-polarization in the transmitted current.

The results for all possible individual symmetry operations are summarized in Table 1, where the identities between spin-resolved conductance terms for which the polarity is reversed (induced by anti-unitary and electrodes-permuting unitary symmetries) have also been included. As can be observed, time-reversal symmetry Θ imposes no restriction on the polarization, although it does impose restrictions on the spin-resolved conductance terms in combination with any spatial symmetry that permutes the electrodes. It does, however, force the oddness (10) of the polarization (1) in combination with particle-hole symmetry (in the exceptional cases in which it holds^{54,55}) with respect to the zero of energy that the latter defines. And, perhaps more importantly, time-reversal symmetry guarantees the vanishing of the whole polarization vector, at all energies at which the final electrode has only one mode¹⁵ (see *Methods*).

Metallic nanocontacts

Nanocontacts are the simplest possible systems in which the previous discussion on spin-polarization can be applied. As shown in Fig. 1, these typically consists of two crystalline fragments or electrodes, source and drain, in contact and placed so that their principal symmetry axes are coincident¹. We consider three different pairs of identical electrodes, all of them presenting a crystallographic cubic system in the bulk, and with the main symmetry axis coincident with a $\langle 001 \rangle$ (4-fold axis), $\langle 111 \rangle$ (3-fold axis), $\langle -110 \rangle$ (2-fold axis) direction of the cubic structure. These are respectively shown in Fig. 1a, 1b, 1c. Metallic, non-magnetic structures of such kind can experimentally be made of Au (FCC), Pb (FCC) or W (BCC), among other elements, including the perfect crystallographic atomic arrangement⁵⁶.

Once the point group \mathcal{G} of the structure is known, one can immediately foresee whether spin-polarization of the transmitted current is possible. According to our previous discussion, the resulting current in systems with groups C_{nv} , D_{nh} , D_{nd} ($n \geq 2$) must be spin-unpolarized. As can be observed in Fig. 1, a simple way of reducing the otherwise high symmetry of a system (for aligned electrodes) is to rotate one electrode while keeping the other fixed. This action preserves all longitudinal rotation symmetries, but in general removes the longitudinal mirror planes (except if the rotation is by an integer multiple of the dihedral angle π/n , with n corresponding to one of the previously mentioned groups); thereby reducing \mathcal{G} to a subgroup² and allowing for a finite polarization at least in the longitudinal direction. Of course, it is not necessary to identify the whole point group of the system in order to rule out spin-polarization; it suffices to look for rotational and mirror symmetries that do not permute the electrodes.

Molecular junctions

In complete analogy with the relative rotation of the electrodes, the placement of a molecule (or, in general, a piece of material) between the contacts either leaves \mathcal{G} invariant or turns it into one of its subgroups, since it obviously cannot add any symmetry that was not already present in the standalone pair of electrodes. As a result, the qualitative effect of adding the molecule to the system is a potential lifting of symmetry-induced restrictions on the spin-resolved conductance and spin-polarization. In particular it may allow for an otherwise forbidden finite polarization, but it cannot cancel it if the bare electrodes already exhibited a non-vanishing polarization.

The spin-resolved conductance, and hence the spin-polarization, can be related with those of an alternative system obtained by application of an orthogonal transformation. If such an operation is a symmetry of the system, then the previous analysis applies and one may find restrictions for these quantities. If, however, the transformation does not leave the system invariant, then by a similar procedure one may relate the conductance terms and polarization of the two systems by equation (13). In particular, the spin-polarization of the transmitted current across a chiral molecule and across its enantiomeric partner may differ only in sign (14), as long as the connection of the enantiomer molecule with the electrodes is done in such a way that the mirror plane which relates both molecules is separately a symmetry of the two electrodes. This topic is elaborated in the *Junctions with chiral molecules* section.

¹The relations in Table 1 would hold for an arbitrary arrangement of the two electrodes, but then all rotational symmetries would necessarily permute them. The case we consider here allows one to obtain the largest possible point groups \mathcal{G} for a two-electrode system.

²Up to isomorphism, as between D_{3d} and D_{3h} in Fig. 1b.

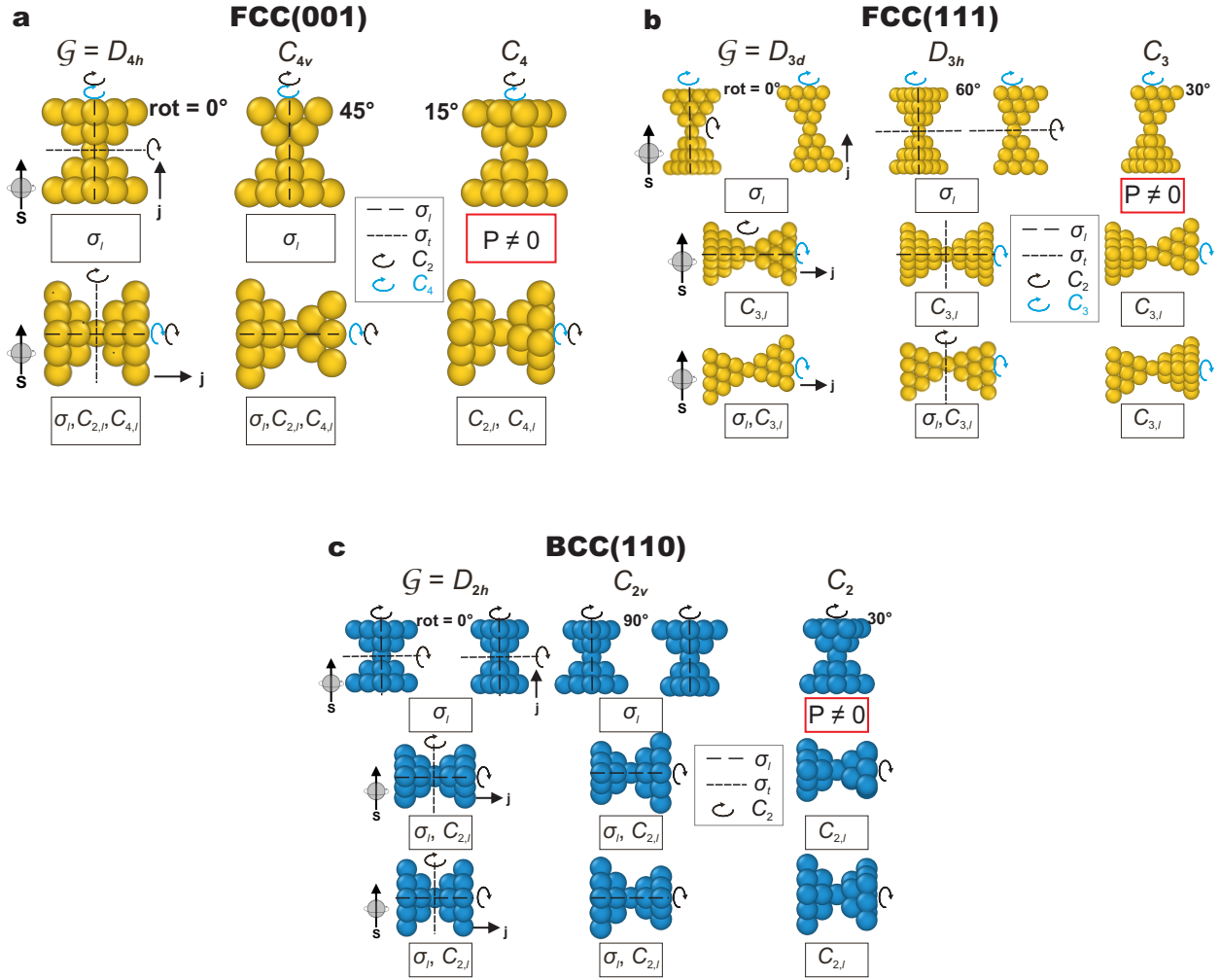


Figure 1. Representative examples of metallic nanocontacts. Rotation angles of the drain electrode (with respect to the source one, ordering indicated by the current direction \mathbf{j}) vary across columns, and the orientation of the electrodes with respect to the spin quantization axis, indicated by \mathbf{s} and with fixed direction here, vary across rows. The point groups \mathcal{G} of the corresponding systems are indicated above each column. Relevant symmetry operations (including a set of generators of the corresponding groups) are explicitly indicated, and those that force the vanishing of the spin-polarization component along \mathbf{s} are indicated in the boxes below each figure, following the notation of Table 1. For the polarization in transversal directions, σ_l is the longitudinal symmetry plane which is parallel to the page. Red boxes with no symmetry operations indicate a finite polarization component instead. **a**, FCC(001) nanocontacts (e.g. Au) with 0°, 45° and 15° electrode relative rotations. **b**, FCC(111) nanocontacts (e.g. Au) with 0°, 60° and 30° relative rotations. **c**, BCC(-110) nanocontacts (e.g. W) with 0°, 90° and 30° relative rotations.

Numerical verification through DFT-based quantum transport calculations

Bare Au, Pb and W nanocontacts

The predictions in Fig. 1 can be verified by means of SOC-corrected DFT quantum transport calculations as implemented in our code Atomistic NanoTransport (ANT.Gaussian)^{57–60}. See the *Supplementary Information (SI)* for further details. Specifically, we show in Fig. 2 that a (longitudinal) mirror symmetry breaking is sufficient to produce a rather large spin-polarization in strong-SOC metal nanocontacts, with Au, Pb and W as our representative elements. To this end we rotate the drain electrode of the nanocontact by an angle θ in increments of 15° and compute the polarization along the longitudinal direction according to equation (1). The energy is fixed at the value in the (−3, 3) eV range that maximizes the maximum

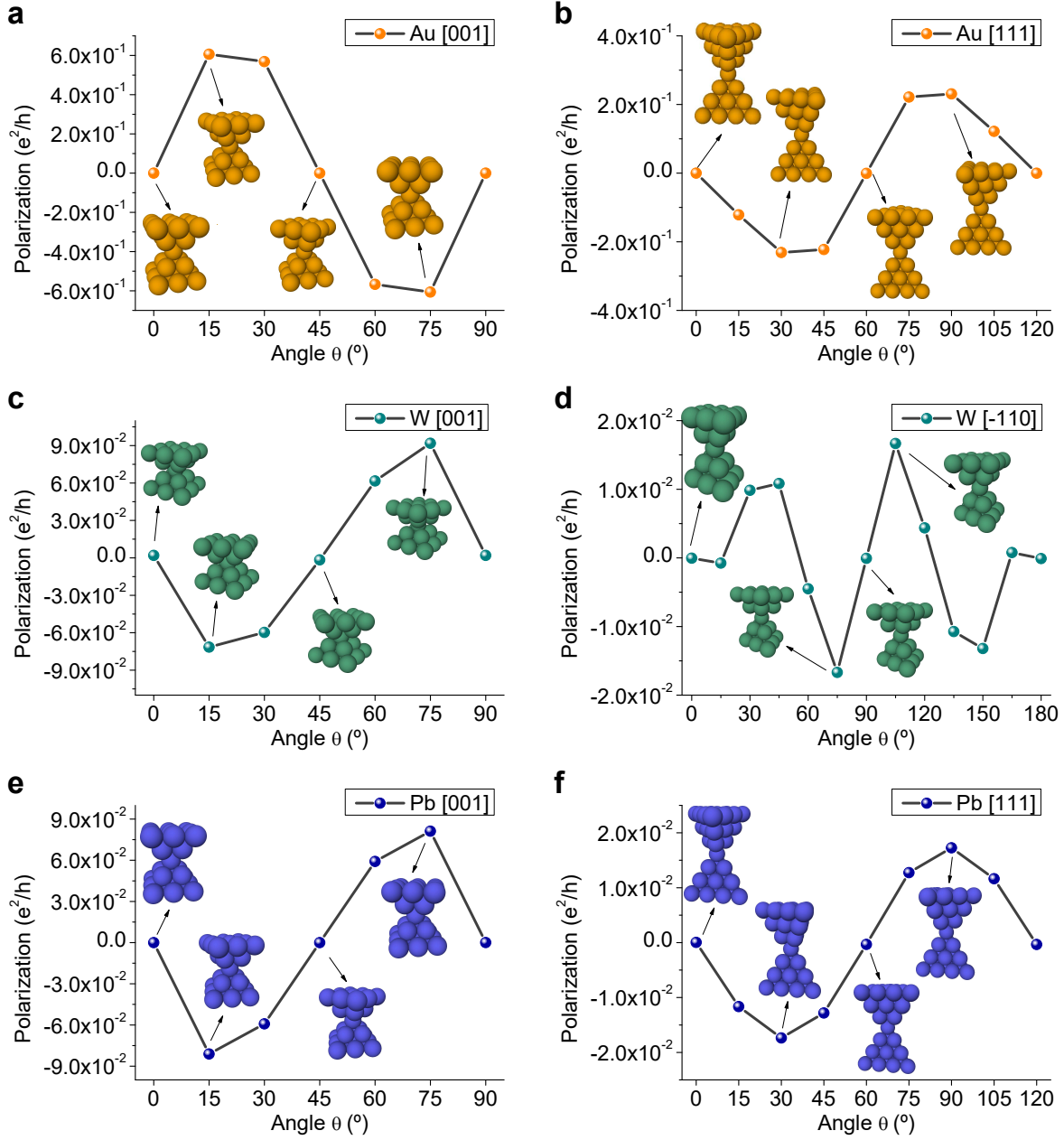


Figure 2. DFT-computed zero-bias spin-polarization (I) along the direction of transport as a function of the angle of relative rotation between the electrodes (only the top half is rotated), at the fixed energy that maximizes the maximum absolute value of spin-polarization across both energies and angles. The oddness of the polarization with respect to the dihedral angles fits nicely into the CISS phenomenology, each pair of systems with opposite polarization being related by a longitudinal mirror plane. **a**, Au(001), point group $\mathcal{G} = D_{4h}$ at $\theta = 0$. **b**, Au(111), D_{3d} at $\theta = 0$. **c**, W(001), D_{4h} at $\theta = 0$. **d**, W(-110), D_{2h} at $\theta = 0$. **e**, Pb(001), D_{4h} at $\theta = 0$. **f**, Pb(111), D_{3d} at $\theta = 0$.

absolute value of polarization across the selected angles³. The maximum θ corresponds to the symmetry operation $C_{n,l} \in \mathcal{G}$ ($\theta = 2\pi/n$), with $n = 4$ in Figs. 2a, 2c, 2e, $n = 3$ in 2b, 2f and $n = 2$ in 2d. The $C_{n,l}$ symmetry guarantees that the displayed curves are $2\pi/n$ -periodic.

The point group \mathcal{G} at each rotation angle can be inferred directly from Fig. 1. At $\theta = \pi/n$, that is, the dihedral angle of

³This maximum occurs at different energy values for the different elements and configurations, depending on the orbital nature of the conductance channels. In particular for Au the maximum occurs below the Fermi energy, where the contribution of the d orbitals kicks in, with zero polarization at the Fermi energy. In contrast, a finite polarization (not the maximum one) at the Fermi energy is obtained for Pb and W. See the SI.

the corresponding \mathcal{G} at $\theta = 0$, the system recovers the longitudinal mirror planes and so the polarization is again vanishing. Importantly, for any two angles $\theta = \pi/n \pm \alpha$ (or more generally, $\theta = m\pi/n \pm \alpha, \forall m \in \mathbb{Z}$) the corresponding systems are related by a longitudinal mirror plane, that is, each arrangement of electrodes transforms into the other by application of a reflection σ_l to the whole system. In this case, for α not an integer multiple of π/n the systems are chiral, one being the enantiomorph of the other. This is a simplified case of the situations with achiral and chiral molecules which are treated below, see Figs. 3 and 4, but the results (14) are the same: *any two systems that can be obtained from one another by a reflection across a plane that does not permute the electrodes present opposite spin-polarization in the direction of propagation*. In fact, the assertion is true for any direction contained in the plane. This phenomenon can be thought of as a generalization of the CISS effect, in the sense that the spin-polarization along the direction of transport vanishes if the system presents such a plane of symmetry, which is forbidden by chirality. In the context of Fig. 2, the polarization–angle curves are hence π/n –antiperiodic when for some θ there is at least one longitudinal mirror plane in \mathcal{G} .

From Fig. 2 it follows that Au exhibits the greatest spin-polarization among the chosen materials, albeit the values with W and Pb nanocontacts are also significant. For all three metals, the 4–fold nanocontacts noticeably exhibit the largest polarization (across all rotation angles), as compared to the 3–fold ones.

Therefore, standalone metal nanocontacts with strong SOC can exhibit significant spin-polarization along the direction of transport due to the symmetry reduction induced by a simple continuous transformation: a rotation of one electrode with respect to the other. This result is reminiscent of the Rashba-Edelstein effect, e.g., as reported in graphene^{7,54} and other 2D crystals⁶, although, to our knowledge, novel in this context.

Junctions with achiral molecules

Achiral molecules, such as benzene or polycyclic aromatic hydrocarbons (in our case a three-ring polybenzenoid, or “triangulene”, with a 3–fold rotation axis), can still give rise to significant spin-polarization when the entire molecular junction, electrodes plus molecule, breaks longitudinal spatial symmetries. This is demonstrated for particularly interesting configurations in Fig. 3 via DFT quantum transport calculations, in analogy with Fig. 2 but as a function of energy and for several rotation angles of the molecule (keeping both electrodes fixed). Unlike previous studies^{39,40}, here SOC is only considered in the metallic electrodes and ignored in the molecules, which emphasizes that the qualitative role of the molecule is purely geometrical.

The introduction of a molecule between the electrodes potentially removes longitudinal rotation and mirror symmetries from the point group \mathcal{G} of the system, the latter depending on the rotation angle of the molecule with respect to the electrodes. The presence of these symmetries forced the spin-polarization to vanish along the corresponding axes (see Table 1) in the systems of standalone electrodes (see Figs. 1, 2). Hence the qualitative effect of the addition of the molecule in the polarization–energy curves is similar to that of the relative rotation of electrodes⁴, further allowing to break longitudinal rotation symmetries.

The importance of the exact position of the molecule on the spin-polarization is apparent from all cases in Fig. 3. For the discrete set of rotation angles that make the longitudinal (regarding the connection to the contacts) symmetry planes of the achiral molecule coincident with the longitudinal symmetry planes of both electrodes, \mathcal{G} contains some σ_l and so the longitudinal spin-polarization is vanishing at all energies, see the blue curve in each subfigure. For any other rotation angle of the molecule, the separately achiral components constitute a chiral system. The longitudinal polarization at any energy is thus reversed between any pair of angles $m\pi/\text{lcm}(n_{\text{el}}, n_{\text{mol}}) \pm \alpha$, with $m \in \mathbb{Z}$, lcm denoting the least common multiple of two integers, and $n_{\text{el}}, n_{\text{mol}} \geq 1$ the number of longitudinal planes of the electrodes and molecule, respectively. This is because the resulting systems are enantiomorph pairs, in analogy with the bare nanocontacts configurations in Fig. 2. In particular, $\text{lcm}(n_{\text{el}}, n_{\text{mol}}) = \text{lcm}(4, 2) = 4$ in Figs. 3a, 3b, $\text{lcm}(3, 2) = 6$ in Fig. 3c and $\text{lcm}(3, 3) = 3$ in Fig. 3d. More compactly, the longitudinal polarization at any energy will be $\pi/\text{lcm}(n_{\text{el}}, n_{\text{mol}})$ –antiperiodic in the rotation of the molecule alone, since the latter is achiral (assuming that the bare pair of electrodes presents any longitudinal mirror symmetry and that it extends to the whole junction for some connection of the molecule); hence the corresponding function is $2\pi/\text{lcm}(n_{\text{el}}, n_{\text{mol}})$ –periodic.

The insets in Figs. 3a, 3b, 3d demonstrate the vanishing of the transversal polarization at all energies due to $C_{2,l}, C_{2,l}, C_{3,l}$ symmetries (at least for the angles that yield the smaller point groups, as specified in the caption, which lack longitudinal mirror planes), respectively. The numerical values obtained in these cases were below the computational error threshold.

As stated above, inversion symmetry is compatible with a finite spin-polarization in the two-terminal device. This is numerically exemplified in Fig. 3a for the angles at which $\mathcal{G} = C_{2h}$, a group that allows for a non-null longitudinal polarization. The point groups containing inversion symmetry that do not force a vanishing polarization, listed in *Symmetry considerations*, are somewhat elusive with standard electrode choices unless an appropriate symmetry-breaking molecule (removing all transverse rotation symmetries or the transverse mirror plane while keeping inversion symmetry), is introduced into the

⁴The quantitative effect, however, is in general completely different. Specific finite values of spin-polarization can vary greatly depending on the molecular energy levels and their orbital character. This can be seen in Fig. 3c where a finite polarization appears at the Fermi energy despite of the use of Au electrodes. The presence of molecular states at the Fermi energy is due to the zero-gap degenerate nature of the triangulene spectrum, since open-shell calculations have not been considered here for simplicity⁶¹.

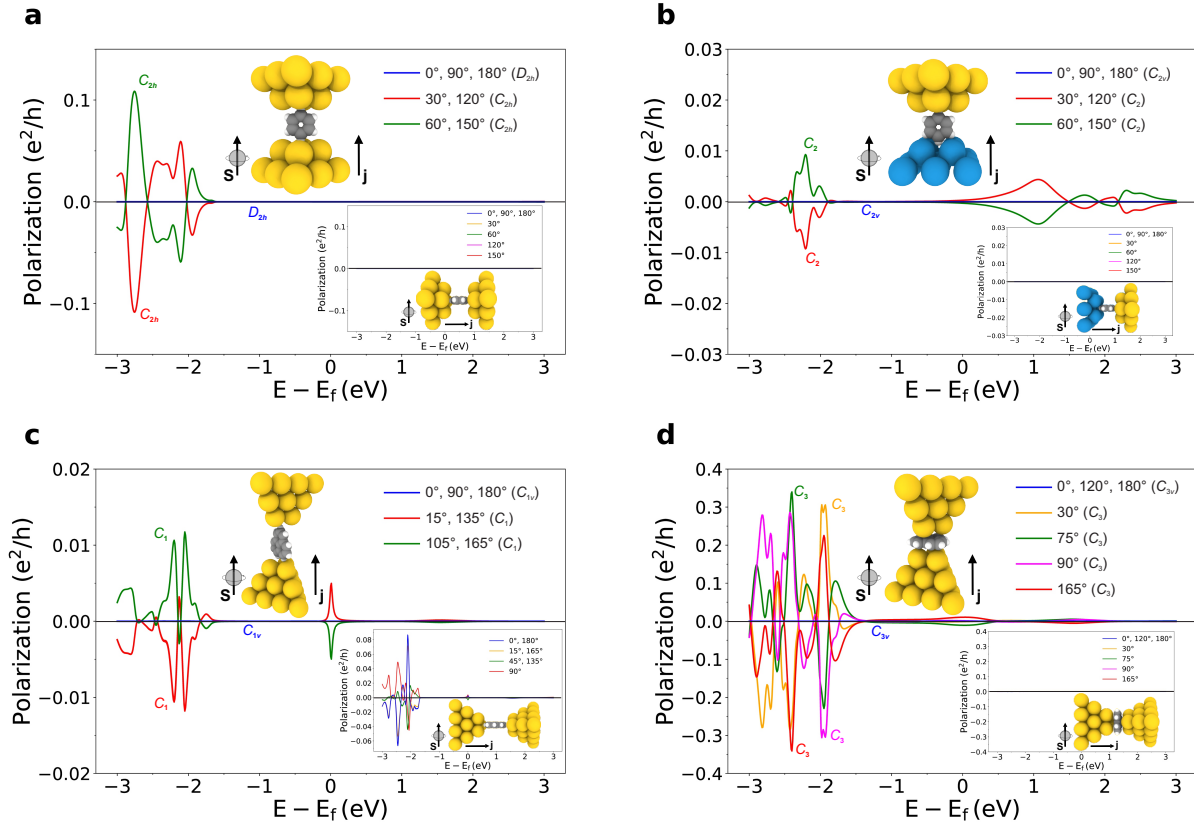


Figure 3. DFT-computed zero-bias spin-polarization (1) along the longitudinal and a transversal direction (the latter shown in the insets), as a function of energy and for different arrangements involving achiral molecules. In all cases the direction of propagation and the polarization component are respectively indicated by \mathbf{j} and \mathbf{s} (insets thus corresponding to transversal polarization of the original structures). The angles correspond to rotations of the molecule alone, along the longitudinal direction. SOC is considered only on the metallic electrodes. **a**, Au(001) electrodes with a parallel benzene (main rotation axis perpendicular to the current direction). **b**, Source W(001) and drain Au(001) electrodes with a parallel benzene. **c**, Au(111) electrodes with a parallel triangulene. **d**, Au(111) electrodes with a triangulene perpendicular to the current direction. The corresponding point groups of the junctions are indicated in the figures. In **a**, **b** and **d**, the vanishing of the transversal polarization for all energies at the angles with lower symmetry is respectively induced by $C_{2,i}$, $C_{2,i}$ and $C_{3,i}$ symmetries. Note that the longitudinal polarization in **a** is non-vanishing even in the presence of inversion symmetry $I_s \in C_{2h}$.

system. This may disguise the fact that inversion symmetry (or the geometrical breaking thereof) is qualitatively irrelevant for spin-polarized transport.

It is worth noting that the vanishing of the spin-polarization in Fig. 3a above approximately -2.5 eV is due to the exclusive s -orbital character of the bulk Au(001) bands in that energy range, see the *SI*. Being proportional to the $\mathbf{L} \cdot \mathbf{S}$ operator, SOC is therefore not present in the system at these energies and so the current must be spin-unpolarized, see *Methods*. In contrast, the W(001) electrode in Fig. 3b does not share this peculiarity, hence enabling spin-polarization in the previous energy range. Nevertheless, depending on where the energy levels of the molecule lie relative to the Fermi level of the junction, it may be possible to observe spin-polarized current at accessible energies (bias voltages) in experimental molecular junctions even with Au contacts (see Fig. 3c). In the case of W or Pb electrodes, the chance is greatly enhanced of always detecting a finite signal at bias voltages on the order of a few hundred mV.

Junctions with chiral molecules

In the following we consider left- and right-handed chiral molecules which make up enantiomeric pairs. Specifically, these molecules are helices made out of a carbon chain and, even though they are not true helicenes²⁴, for simplicity we refer to them as such. These have been used in previous theoretical studies of the CISS effect^{39,40} and we consider here two variants (along

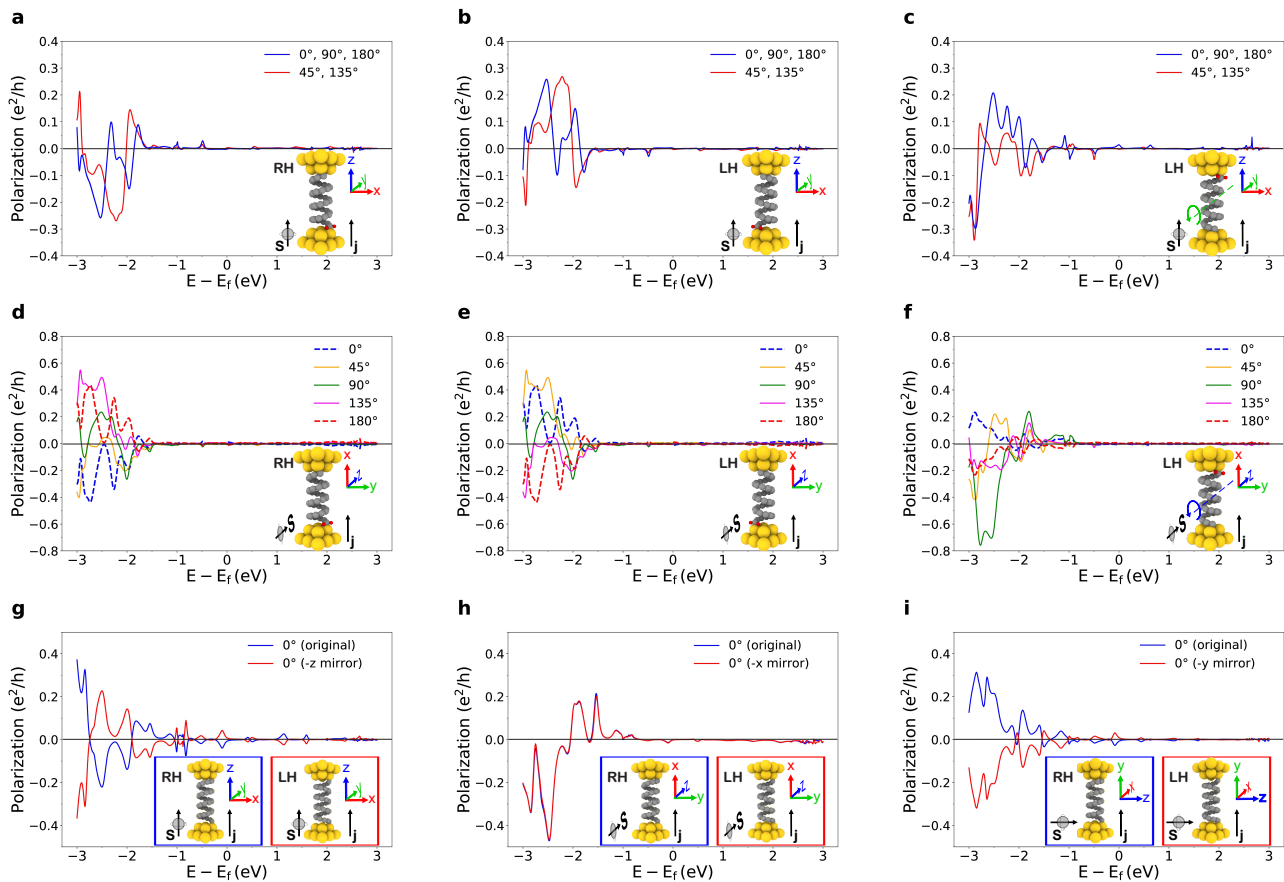


Figure 4. DFT-computed zero-bias spin-polarization (I) along the longitudinal and transversal directions, as a function of energy and for different arrangements involving chiral molecules, in particular two types of helicenes (see the main text). In all cases, z and s indicate the corresponding polarization component. The angles correspond to rotations of the molecule alone, along the longitudinal direction. SOC is considered only on the metallic electrodes, which are Au(001) in all cases. **a**, Asymmetric helicene; longitudinal polarization. **b**, Its enantiomeric partner connected such that the system is the specular reflection of **a** through a (centred) longitudinal plane; longitudinal polarization. **c**, Analogous to **b**, but with the connection of the enantiomer realized through a reflection on the (centred) transversal plane; longitudinal polarization. **d**, **e**, **f**, Analogous to **a**, **b**, **c** respectively, but for transversal polarization (spins point into the page as the perspective in the insets suggests). Point group of the junctions in **a-f**: $\mathcal{G} = C_1$ (trivial). **g**, Symmetric helicene with the transversal rotation $C_{2,x}$. Original (blue) and enantiomeric partner (red) connected such that the system is the specular reflection of the original one through the transversal plane; longitudinal polarization. **h**, Analogous to **g**, but for transversal polarization in a direction perpendicular to the C_2 symmetry axis. **i**, Analogous to **g**, but for transversal polarization in a direction parallel to the C_2 symmetry axis. Point group of the junctions in **g-i**: $\mathcal{G} = C_2$, with transversal orientation. LH and RH refer to left- and right-handed enantiomers, respectively. The longitudinal spin-polarization is reversed between enantiomeric pairs as long as both systems as a whole (including the nanocontacts) are related by reflection through a plane that does not permute the electrodes (**a,b**). This is also true for the transversal polarization component contained in such plane (**d,e**), while the transversal component normal to it remains invariant. If the enantiomeric partner is connected according to a transversal plane, the polarization is altered unpredictably (**c,f**) unless the molecule has a 2-fold transversal rotation symmetry, in which case both connections of the enantiomer are identical (**g-i**).

with their respective enantiomeric partners)⁵, the first (asymmetric helicene) being a molecule with no spatial symmetries and depicted in Figs. 4a - 4f, the second (symmetric helicene) presenting just a 2-fold transversal rotation symmetry and employed

⁵The molecule has been taken from the supplementary material of Zöllner et al.⁴⁰ and modified in two ways. Technically, the original molecule lacks any unitary symmetry, but, in a way, it is not far from having a 2-fold transversal rotation symmetry $C_{2,t}$ (perpendicular to the axis of the helix). In Figs. 4a - 4f the hydrogen atoms and two carbon atoms from one end have been removed in order to make the molecule “more asymmetric”. In contrast, the molecule exhibits the $C_{2,t}$ symmetry in Figs. 4g - 4i due to the removal of the hydrogen atoms from both ends.

in 4g - 4i.

As shown in Figs. 3 and 4a, 4d and proved in equation (15), a longitudinal rotation of the molecule changes the spin-polarization along any direction in an unpredictable way, except for a discrete set of angles determined by the symmetries of the molecule and electrodes (see equation (13) and the discussion thereafter). It is then to be expected that a variation in the anchoring of the enantiomeric partner between the contacts also has an unpredictable effect on the polarization. By equation (14), however, the two sets of polarization–energy curves (along a given direction) obtained from the pair of molecules have a one-to-one correspondence, given by a reversal of sign at least along the longitudinal direction according to equation (14). This reversal of the spin-polarization, which accounts for the CISS effect, occurs when the enantiomeric partner junction is realized through the application of a mirror symmetry of both electrodes, turning one system into another (enant₁ in *Methods*). These two junctions are shown in Figs. 4a, 4b. Even if the relative longitudinal rotation angle between the molecule and its enantiomeric partner could not be controllable in practice, the average spin-polarization over different connections (varying this angle) of both molecules would tend to be the opposite of each other. While for the longitudinal direction the average spin-polarization will in general be a finite value (unlike for achiral molecules if \mathcal{G} contains any longitudinal mirror symmetry), for any transversal direction the average will always tend to zero since the polarization at any given energy is π -antiperiodic due to equation (14)⁶. This is illustrated in Figs. 4d, 4e.

This way of realizing the enantiomeric partner junction (up to longitudinal rotations), namely, through longitudinal mirror symmetries of the electrodes, yields, to an extent, a familiar result. In contrast, if the connection of the enantiomeric partner is realized through a reflection on the transversal plane (enant₂ in *Methods*), by equation (15) the spin-polarization will in general not be related to that of the original molecule, even if longitudinal rotations are considered. This is displayed in Figs. 4c, 4f. Note that it has been implicitly assumed in these general discussions that the standalone electrodes present the corresponding planes of symmetry, for which Figs. 1 and 2 may be used as a guide.

Both ways of realizing the enantiomeric partner connection (up to longitudinal rotations) are qualitatively different due to the absence of a 2-fold transversal rotation of the molecule. The spin-polarization of the enantiomeric partner junction obtained through the transversal plane σ_t will be equal to that obtained through a longitudinal plane σ_l if the molecule presents the aforementioned rotation symmetry and it is placed with the appropriate longitudinal angle such that the rotation symmetry is shared by the electrodes, i.e., $C_{2,t} = \sigma_l \sigma_t \in \mathcal{G}$. This is exemplified in Figs. 4g- 4i, where the symmetries are respectively $C_{2,x}, C_{2,y}, C_{2,z} \in \mathcal{G}$ (shared by the electrodes and chiral molecule). The “transversal” enantiomeric partner (analogous to that in Figs. 4c, 4f and displayed in the red panels) is identical to that obtained through a reflection on a longitudinal plane, as it should be since $\sigma_t = \sigma_l C_{2,t}$ and $C_{2,t} \in \mathcal{G}$ is a symmetry of the system; and so is the resulting polarization. The invariance (reversal) of the polarization of the enantiomeric partner in Fig. 4h (4i) occurs due to the geometrical equivalence between inverting the longitudinal coordinate and the spin direction \hat{z} (the transversal direction normal to \hat{z} , respectively), see equation (16).

Outlook

The lack of certain symmetry planes is the distinctive feature of chiral molecules regarding their potential to induce spin-polarized transport in molecular junctions, irrespective of the specific shape of the former; helix-like or not (which may nevertheless play an important quantitative role). This idea has been here taken a step further, extending the concept of chirality in the CISS effect to the junction as a whole and providing the following generalization: any two systems obtained from one another by the reflection through a plane that does not permute the electrodes present opposite spin-polarizations along the direction of transport. In particular, systems that are left invariant under such a reflection cannot induce a finite polarization along that direction, in agreement with the traditional CISS concept. The inevitable breaking of these symmetry planes in junctions with chiral molecules makes the use of them a sufficient, but not necessary condition to observe the spin-polarization.

Our theoretical predictions have been confirmed by non-magnetic DFT electronic transport calculations for standard nanocontacts with strong SOC and several prototypical achiral and chiral molecules, which could be employed in actual experimental configurations. In particular, a simple rotation of any component of the junction, molecule (if present), drain, or source electrode will generally induce spin-polarization along the direction of transport due to the breaking of the mirror symmetry planes that do not permute the electrodes. This feature may be exploited to mechanically switch between polarized and unpolarized currents in the same device, something that cannot be accomplished with permanent ferromagnetic elements.

At a quantitative level, our DFT results for FCC Au nanocontacts with or without molecules, show that for finite bias voltages near the Fermi level, Au will not, as expected, exhibit measurable spin-polarization unless an organic molecule with frontier *p*-orbitals near the Fermi level is included in the junction. On the other hand, we predict that FCC Pb and BCC W electrodes may exhibit non-negligible spin-polarization near the Fermi level, and thus at low bias voltages in experiments. In any case, even if the presence of a molecule is not needed to generate a finite spin-polarization, they can still be crucial to explain the rather large measured values^{31,62}.

⁶A longitudinal π -rotation of the molecule is equivalent to the reversal of the transversal direction from which the spin-polarization is measured, if that is a symmetry of the electrodes.

It is worth to note that, in practice, the symmetry of the system may be reduced by defects. As is customary in solid-state physics, group-theoretical results are then being understood as a limiting case, and in particular the spin-polarization would be expected to be small, but not strictly vanishing, if the deviation from the suitable, perfectly symmetrical configuration is small. Nevertheless, the reduction of symmetry plays in favor of a finite spin-polarization.

Notice that our symmetry-based analysis and DFT calculations allow us to predict and quantify essential features of the spin-polarization of the current in non-magnetic two-terminal devices. We have not addressed here how to actually verify the predicted spin-polarization, as defined through (1), in the laboratory. This would certainly require the inclusion of more elements in the circuit such as magnetic electrodes, additional terminals, nodes where spin accumulation can be measured, finite bias, or dephasing^{37,38}. This is a discussion beyond the current scope of our work, but important nevertheless when it comes to a practical use of the CISS effect. Regardless, a finite spin-polarization, as defined by (1), is an essential requirement as part of any more complex circuit to be of any use in spintronics applications.

Methods

Symmetry analysis

Note: in this work we assume the existence of a single longitudinal direction which acts as a symmetry axis for both electrodes separately, and along which electronic propagation takes place. Most of the analysis in this section would still hold for an arbitrary arrangement of the electrode pair, particularly equations (2)-(8), (13); but care should be taken when cataloging the possible symmetries of the system and the directions of spin quantization axis for which the spin-polarization is qualitatively affected by them.

Electronic transport in a system with two leads can be formulated as a scattering problem between eigenstates of the isolated electrodes^{15,16,37,42,63-68}. At a given energy E , let α_i, α'_i ($i = 1, \dots, M_A$) be the incoming and outgoing (with respect to the scattering region) modes of electrode A , and β_j, β'_j ($j = 1, \dots, M_B$) the outgoing and incoming modes of electrode B . These modes label the eigenstates ψ^α, ψ^β , which are in general spinors, of the corresponding isolated electrode which are normalized to carry unit current⁷. The spin-resolved conductance between the leads A (initial) and B (final) can then be defined in terms of the scattering matrix elements as:

$$G_{s',s}^{AB}(E) = \frac{e^2}{h} \sum_{i=1}^{M_A} \sum_{j=1}^{M_B} |S_{s',s}^{\beta_j \alpha_i}|^2 = \frac{e^2}{h} \sum_{i=1}^{M_A} \sum_{j=1}^{M_B} \left| \langle \psi_{s'}^{\beta_j} | \hat{S} | \psi_s^{\alpha_i} \rangle \right|^2 = \frac{e^2}{h} \sum_{i=1}^{M_A} \sum_{j=1}^{M_B} \left| \int_{\mathbb{R}^3} \psi_{s'}^{\beta_j}(\mathbf{r})^* \hat{S}(\mathbf{r}) \psi_s^{\alpha_i}(\mathbf{r}) d^3 \mathbf{r} \right|^2 \quad (2)$$

where $s, s' \in \{\uparrow, \downarrow\}$ respectively label the initial and final spin states, or spinor components, referred to a given direction of quantization and \hat{S} is the unitary scattering operator^{69,70}. This is consistent with the so-called spin polarizer picture⁴⁶. The energy and electrodes labels will be dropped for simplicity, except when mandatory. \hat{S} depends on the spatial coordinates \mathbf{r} exclusively via the Hamiltonian of the complete system, which includes the scattering region formed by the contacts (or part of the leads which is sufficiently close to the scattering region) plus, possibly, a molecule or piece of material between them. For an incident unpolarized current, the component of the spin-polarization (of the outgoing current) along an arbitrary spin quantization axis reads¹⁶, up to a normalization factor:

$$P = G_{\uparrow\uparrow} + G_{\uparrow\downarrow} - G_{\downarrow\uparrow} - G_{\downarrow\downarrow} ,$$

where the \uparrow, \downarrow spin states are again referred to the spin quantization axis. The whole polarization vector \mathbf{P} may then be evaluated by rotating the spin axis and applying (1), which is the method here employed in numerical calculations with `ANT.Gaussian`. Analogously, for a fixed quantization axis along \hat{z} one may compute the perpendicular components as¹⁶:

$$P_x = \frac{2e^2}{h} \sum_{i=1}^{M_A} \sum_{j=1}^{M_B} \text{Re} \tilde{P}, \quad P_y = \frac{2e^2}{h} \sum_{i=1}^{M_A} \sum_{j=1}^{M_B} \text{Im} \tilde{P}, \quad \tilde{P} \equiv S_{\uparrow\uparrow}^{\beta_j \alpha_i} S_{\downarrow\uparrow}^{\beta_j \alpha_i} + S_{\uparrow\downarrow}^{\beta_j \alpha_i} S_{\downarrow\downarrow}^{\beta_j \alpha_i}$$

with \hat{x}, \hat{y} the directions along which the Pauli vector has components σ_x, σ_y (in the usual representation) respectively.

In the case of no spin-dependent terms (originating from SOC or non-collinear magnetism), anywhere in the contacts or molecules, then it must be $S_{\uparrow\uparrow}^{\beta_j \alpha_i} = S_{\downarrow\downarrow}^{\beta_j \alpha_i}$, $S_{\uparrow\downarrow}^{\beta_j \alpha_i} = S_{\downarrow\uparrow}^{\beta_j \alpha_i} = 0$, so that all the polarization components are vanishing. In our case, the metallic contacts present strong SOC and we ignore it in the molecules, as in practice it is negligibly small in light elements.

⁷We have implicitly assumed that both electrodes present time-reversal or inversion symmetry, so that at any energy in each electrode the number of incoming modes coincides with the number of outgoing modes (for crystalline electrodes, this is due to the evenness of the energy spectrum in the Brillouin zone). Nevertheless, only the analysis of anti-unitary symmetries requires that condition; the rest would be analogous.

Spatial (unitary) symmetries

Let $\mathcal{G} \subset O(3)$ be the point group of the complete system. Then $\hat{S}(g^{-1}\mathbf{r}) = \hat{S}(\mathbf{r})$ for any spatial symmetry operation $g \in \mathcal{G}$, and owing to the invariance of the integral under this coordinate transformation⁷¹:

$$S_{s',s}^{\beta_j\alpha_i} = \sum_{s_1,s'_1} \mathcal{D}^{1/2}(g)_{s',s'_1} \mathcal{D}^{1/2}(g)_{s,s_1}^* \int_{\mathbb{R}^3} (\bar{g}\psi_{s'_1}^{\beta_j}(\mathbf{r})^*) \hat{S}(\mathbf{r}) (\bar{g}\psi_{s_1}^{\alpha_i}(\mathbf{r})) d^3\mathbf{r}, \quad \forall g \in \mathcal{G} \quad (3)$$

where \bar{g} denotes the action of the coordinate transformation g on the spinor functions which does not affect its (spin) components, and $\mathcal{D}^{1/2}$ is the (projective) representation of $O(3)$ of angular momentum $1/2$, given by

$$\mathcal{D}^{1/2}(C_\theta) = \pm \mathcal{D}^{1/2}(I_s C_\theta) = e^{i\boldsymbol{\sigma}\hat{\mathbf{e}}\theta/2} = \begin{pmatrix} a & b \\ -b^* & a^* \end{pmatrix}, \quad a = \cos(\theta/2) + ie_z \sin(\theta/2), \quad b = (e_y + ie_x) \sin(\theta/2) \quad (4)$$

for a θ -rotation along direction $\hat{\mathbf{e}}$, where $\boldsymbol{\sigma}$ is the Pauli vector and the parity under inversion I_s has been dropped from the notation since it does not affect equation (2) or (1). This representation carries the transformation of the spinor components under an operation $g \in \mathcal{G}$, and the particular form we have given is valid under the assumption that the spin is projected along $\hat{\mathbf{z}}$; otherwise an orientation-preserving change of coordinates is needed to determine $\hat{\mathbf{e}}$.

At this point we must distinguish two cases among the symmetry operations $g \in \mathcal{G}$. Let \mathcal{G}_A (\mathcal{G}_B) be the point group of the isolated electrode A (B , resp.) with the same fixed point as \mathcal{G} :

- g is a symmetry for each electrode in isolation, that is, $g \in \mathcal{G}_A \cap \mathcal{G}_B$. Then g cannot affect the longitudinal coordinate and thus \bar{g} does not alter the incoming/outgoing nature of the modes, nor their energy. Therefore $\bar{g}\psi^{\alpha_i} = \sum_k \mathcal{D}^{\alpha_i}(g)_{k,i} \psi^{\alpha_k}$ where \mathcal{D}^{α_i} is the representation of \mathcal{G}_A according to which ψ^{α_i} transforms, and an analogous result follows for electrode B . Inserting this in equation (3), it is straightforward to prove (invoking the unitarity of such representations) that $G_{s',s}^{AB}(E)$ is actually independent on all $\mathcal{D}^{\alpha_i}, \mathcal{D}^{\beta_j}$ regardless of their dimensions, hence in this case:

$$G_{s',s}^{AB}(E) = \frac{e^2}{h} \sum_{i=1}^{M_A} \sum_{j=1}^{M_B} \left| \sum_{s_1,s'_1} \mathcal{D}^{1/2}(g)_{s',s'_1} \mathcal{D}^{1/2}(g)_{s,s_1}^* \langle \psi_{s'_1}^{\beta_j} | \hat{S} | \psi_{s_1}^{\alpha_i} \rangle \right|^2, \quad \forall g \in \mathcal{G} \cap \mathcal{G}_A \cap \mathcal{G}_B \quad (5)$$

- g is not a symmetry for each electrode in isolation, that is, $g \notin \mathcal{G}_A \cap \mathcal{G}_B$. Then g , if it exists, necessarily permutes the electrodes, which must thus have identical composition. In this case the longitudinal coordinate is inverted, hence the existence of such a symmetry establishes a one-to-one correspondence (\bar{g}) between the incoming modes $\{\alpha_i\} \leftrightarrow \{\beta'_j\}$ and also between the outgoing modes $\{\beta_j\} \leftrightarrow \{\alpha'_i\}$ ($i, j = 1, \dots, M_A = M_B = M$), so that:

$$G_{s',s}^{AB}(E) = \frac{e^2}{h} \sum_{i,j=1}^M \left| \sum_{s_1,s'_1} \mathcal{D}^{1/2}(g)_{s',s'_1} \mathcal{D}^{1/2}(g)_{s,s_1}^* \langle \psi_{s'_1}^{\alpha'_i} | \hat{S} | \psi_{s_1}^{\beta'_j} \rangle \right|^2, \quad \forall g \in \mathcal{G} \setminus (\mathcal{G}_A \cap \mathcal{G}_B) \quad (6)$$

Therefore we may treat symmetry operations individually irrespective of the groups $\mathcal{G}_A, \mathcal{G}_B$ they belong to. From equations (5), (6) it follows that there will be a relation between the spin elements of G^{AB} or between those of G^{AB}, G^{BA} (respectively) whenever $\mathcal{D}^{1/2}(g)$ has exactly two out of four non-null entries, which occurs for rotations along the spin quantization direction ($b = 0$ in equation (4)) and for π -rotations perpendicular to it ($a = 0$ in equation (4)), or equivalently for reflections through planes perpendicular to these axes.

Anti-unitary symmetries

For non-magnetic systems the group of symmetries is a grey point group, which is constructed from the previous \mathcal{G} by allowing for the time-reversal operation $\Theta = \sigma_y K$, where σ_y acts on the spinor components only and K denotes complex conjugation. Noting that Θ is an anti-unitary operation, that $\Theta \hat{S} \Theta^{-1} = \hat{S}^\dagger$ (in analogy with the time evolution operator) if time-reversal is indeed a symmetry of the Hamiltonian ($\sigma_y H^* \sigma_y = H$, in the time-independent case) and that K inverts the propagation direction of the modes within each electrode (thus making a correspondence $\{\alpha_i\} \leftrightarrow \{\alpha'_i\}$ and $\{\beta_j\} \leftrightarrow \{\beta'_j\}$):

$$G_{s',s}^{AB}(E) = \frac{e^2}{h} \sum_{i=1}^{M_A} \sum_{j=1}^{M_B} \left| \langle \Theta \psi_{s'_1}^{\beta_j} | \Theta \hat{S} \Theta^{-1} | \Theta \psi_{s_1}^{\alpha_i} \rangle^* \right|^2 = \frac{e^2}{h} \sum_{i=1}^{M_A} \sum_{j=1}^{M_B} \left| \sum_{s_1,s'_1} (\sigma_y^*)_{s,s_1} (\sigma_y)_{s',s'_1} \langle \psi_{s_1}^{\alpha'_i} | \hat{S} | \psi_{s'_1}^{\beta'_j} \rangle \right|^2 = G_{\bar{s},\bar{s}'}^{BA}(E) \quad (7)$$

where \bar{s}, \bar{s}' denote the opposite spin states of s, s' , respectively; and we have introduced the conductance G^{BA} from electrode B to A :

$$G_{s',s}^{BA}(E) = \frac{e^2}{h} \sum_{i=1}^{M_A} \sum_{j=1}^{M_B} \left| \langle \psi_{s'}^{\alpha'_i} | \hat{S} | \psi_s^{\beta'_j} \rangle \right|^2$$

Combining equations (6) and (7) we obtain the action of the symmetries $g\Theta$ and Θg on the conductance for any spatial operation g that permutes the electrodes. The result in both cases is:

$$G_{s',s}^{AB}(E) = \frac{e^2}{h} \sum_{i,j=1}^M \left| \sum_{s_1, s'_1} \mathcal{D}^{1/2}(g)_{\bar{s}, s_1} \mathcal{D}^{1/2}(g)_{s', s'_1}^* \langle \psi_{s'_1}^{\beta_j} | \hat{S} | \psi_{s_1}^{\alpha_i} \rangle \right|^2, \quad \forall g \in \mathcal{G} \setminus (\mathcal{G}_A \cap \mathcal{G}_B) \quad (8)$$

which readily allows to obtain the restrictions imposed on G^{AB} by these operations.

Another important consequence of time-reversal symmetry, which was first stated by Zhai and Xu¹⁵ and latter expanded by Utsumi et al.⁶⁸, is the fact that *all spin-polarization components vanish at any energy at which the final electrode has only one mode*, i.e., $M_B = 1$ in our notation. The proof is as follows. Setting $M_B = 1$, by the unitarity of the S matrix:

$$\sum_{i=1}^{M_A} \sum_s S_{s_1, s}^{\beta \alpha_i} S_{s_2, s}^{\beta \alpha_i *} + S_{s_1, \uparrow}^{\beta \beta'} S_{s_2, \uparrow}^{\beta \beta' *} + S_{s_1, \downarrow}^{\beta \beta'} S_{s_2, \downarrow}^{\beta \beta' *} = \delta_{s_1, s_2}$$

and the condition imposed by time-reversal symmetry (note that in this case $\Theta \psi_s^\beta = i(\delta_{s, \uparrow} - \delta_{s, \downarrow}) \psi_s^{\beta'}$):

$$S_{s_1, s_2}^{\beta \beta'} = (2\delta_{s_1, s_2} - 1) S_{\bar{s}_2, \bar{s}_1}^{\beta \beta'} \Rightarrow S_{\uparrow \uparrow}^{\beta \beta'} = S_{\downarrow \downarrow}^{\beta \beta'}, \quad S_{\uparrow \downarrow}^{\beta \beta'} = S_{\downarrow \uparrow}^{\beta \beta'} = 0$$

setting $s_1 = s_2 = s'$, one obtains $G_{s', \uparrow} + G_{s', \downarrow} = G_{\bar{s}', \uparrow} + G_{\bar{s}', \downarrow}$, which implies that $P = 0$ in (1) for every spin quantization axis, hence $\mathbf{P} = 0$ at the corresponding energy.

For completeness we also comment on particle-hole (or charge conjugation) symmetry \mathcal{C} , although it is not present in the physical systems of this work. In our basis, this operator is represented as $\mathcal{C} = IK$, where I is the identity operator acting on the spinor components only. The condition on the Hamiltonian $\mathcal{C}H\mathcal{C}^{-1} = -H$ implies $\mathcal{C} \psi_s^{\alpha_i}(E) = \psi_s^{\alpha'_i}(-E)$, where we have explicitly included the energy (measured from a Fermi level obtained from the previous condition on the Hamiltonian) corresponding to each eigenfunction, and omitted the arbitrary phase factor since it is cancelled in our calculations. Therefore:

$$G_{s',s}^{AB}(E) = \frac{e^2}{h} \sum_{i=1}^{M_A} \sum_{j=1}^{M_B} \left| \langle \mathcal{C} \psi_{s'}^{\beta'_j} | \mathcal{C} \hat{S} \mathcal{C}^{-1} | \mathcal{C} \psi_s^{\alpha_i} \rangle^* \right|^2 = \frac{e^2}{h} \sum_{i=1}^{M_A} \sum_{j=1}^{M_B} \left| \langle \psi_{s'}^{\beta'_j}(-E) | \hat{S}^\dagger(-H) | \psi_s^{\alpha'_i}(-E) \rangle \right|^2 = G_{s',s}^{BA}(-E) \quad (9)$$

By equations (7), (9), the combination $\Theta\mathcal{C}$ would yield the condition:

$$G_{s',s}^{AB}(E) = G_{\bar{s}', \bar{s}}^{AB}(-E) \Rightarrow \mathbf{P}(E) = -\mathbf{P}(-E) \quad (10)$$

However, particle-hole symmetry will rarely be present in realistic systems beyond simplified models. A family of materials which may reasonably exhibit this symmetry are the carbon allotropes^{54,55}.

This exhausts the set of anti-unitary symmetries⁷². Note that for (7)-(10) to be applicable, the whole system needs to have the corresponding symmetry. In particular, placing a non-magnetic molecule or material between magnetic electrodes (or vice-versa) would break the time reversal symmetry of the system.

Application

Equations (5)-(8) determine the symmetry-induced relations on the spin-resolved conductance $G_{s',s}^{AB}$ for a given spin quantization axis, and possibly also on the corresponding spin-polarization component (1), at each energy. These results are summarized in Table 1 for symmetries that are compatible with the 2-lead configuration. Most of them are straightforward to obtain from the previous relations, except perhaps for the longitudinal $2\pi/n$ -rotation $C_{n,l}$ ($n \geq 2$) for any transversal spin projection. Fixing \hat{z} as an arbitrary transversal direction, we may in principle assign any direction in the xy -plane to the longitudinal one, hence we write $\hat{e} = (\sin(\varphi), \cos(\varphi), 0)$, for any $\varphi \in [0, 2\pi)$. Then by equation (4):

$$\mathcal{D}^{1/2}(C_n^m) = \begin{pmatrix} \cos(\pi m/n) & \sin(\pi m/n) e^{i\varphi} \\ -\sin(\pi m/n) e^{-i\varphi} & \cos(\pi m/n) \end{pmatrix}, \quad \forall m = 1, \dots, n-1$$

and by equation (5);

$$\begin{aligned}
G_{\uparrow\uparrow} &= \frac{e^2}{h} \sum_{i=1}^{M_A} \sum_{j=1}^{M_B} \left| \cos(\pi m/n)^2 S_{\uparrow\uparrow}^{\beta_j \alpha_i} + \sin(\pi m/n)^2 S_{\downarrow\downarrow}^{\beta_j \alpha_i} + \cos(\pi m/n) \sin(\pi m/n) \left[e^{i\varphi} S_{\downarrow\uparrow}^{\beta_j \alpha_i} + e^{-i\varphi} S_{\uparrow\downarrow}^{\beta_j \alpha_i} \right] \right|^2, \\
G_{\uparrow\downarrow} &= \frac{e^2}{h} \sum_{i=1}^{M_A} \sum_{j=1}^{M_B} \left| \cos(\pi m/n) \sin(\pi m/n) e^{i\varphi} \left[-S_{\uparrow\uparrow}^{\beta_j \alpha_i} + S_{\downarrow\downarrow}^{\beta_j \alpha_i} \right] - \sin(\pi m/n)^2 e^{i2\varphi} S_{\downarrow\uparrow}^{\beta_j \alpha_i} + \cos(\pi m/n)^2 S_{\uparrow\downarrow}^{\beta_j \alpha_i} \right|^2, \\
G_{\downarrow\uparrow} &= \frac{e^2}{h} \sum_{i=1}^{M_A} \sum_{j=1}^{M_B} \left| \cos(\pi m/n) \sin(\pi m/n) e^{-i\varphi} \left[-S_{\uparrow\uparrow}^{\beta_j \alpha_i} + S_{\downarrow\downarrow}^{\beta_j \alpha_i} \right] + \cos(\pi m/n)^2 S_{\downarrow\uparrow}^{\beta_j \alpha_i} - \sin(\pi m/n)^2 e^{-i2\varphi} S_{\uparrow\downarrow}^{\beta_j \alpha_i} \right|^2, \\
G_{\downarrow\downarrow} &= \frac{e^2}{h} \sum_{i=1}^{M_A} \sum_{j=1}^{M_B} \left| \sin(\pi m/n)^2 S_{\uparrow\uparrow}^{\beta_j \alpha_i} + \cos(\pi m/n)^2 S_{\downarrow\downarrow}^{\beta_j \alpha_i} - \cos(\pi m/n) \sin(\pi m/n) \left[e^{i\varphi} S_{\downarrow\uparrow}^{\beta_j \alpha_i} + e^{-i\varphi} S_{\uparrow\downarrow}^{\beta_j \alpha_i} \right] \right|^2
\end{aligned}$$

Inserting these in equation (1) we obtain, after some algebra:

$$P_z = \cot(\pi m/n) \frac{e^2}{h} \sum_{i=1}^{M_A} \sum_{j=1}^{M_B} \left[e^{i\varphi} \left(S_{\uparrow\uparrow}^{\beta_j \alpha_i*} S_{\downarrow\uparrow}^{\beta_j \alpha_i} + S_{\downarrow\downarrow}^{\beta_j \alpha_i*} S_{\uparrow\downarrow}^{\beta_j \alpha_i} \right) + \text{c.c.} \right] = \cot(\pi m/n) \text{Re} \left[e^{i\varphi} (P_x + iP_y) \right], \quad \forall m = 1, \dots, n-1 \quad (11)$$

where we have introduced the perpendicular components of the spin-polarization ($\hat{\mathbf{z}}$ being the fixed quantization axis, along the chosen transversal direction in this case). Since $\cot(x) = -\cot(\pi - x)$, applying equation (11) for $m = 1$ and $m = n - 1$ (that is, for $C_{n,l}$ and its inverse $C_{n,l}^{-1}$) we conclude that

$$P = 0 \quad \text{along any transversal direction if there exists some } n \geq 2 \text{ such that } C_{n,l} \in \mathcal{G} \quad (12)$$

This result was easy to obtain for $n = 2$ since $\mathcal{D}^{1/2}(C_{2,l})$ has two null entries. In that case $C_{2,l}$ is its own inverse and $\cot(\pi/2) = 0$ readily. For $n \geq 3$, however, it must be $\text{Re}[e^{i\varphi}(P_x + iP_y)] = 0$; which is consistent with the fact that in this case the polarization is a vector along the direction of transport, noting that $\varphi = 0$ ($\pi/2$) if $\hat{\mathbf{y}}$ ($\hat{\mathbf{x}}$, respectively) corresponds to the longitudinal direction.

Rotated systems and enantiomers

Consider now an orthogonal spatial operation which is not a symmetry of the system; $g \notin \mathcal{G}$. Performing the corresponding change of coordinates in equation (2) we obtain a new scattering operator $\hat{S}(\mathbf{r})' = \hat{S}(g^{-1}\mathbf{r}) \neq \hat{S}(\mathbf{r})$ and eigenfunctions $\mathcal{D}^{1/2}(g)^* \psi(\mathbf{r})' = \psi(g^{-1}\mathbf{r})$ (which have the opposite incoming/outgoing nature if and only if g inverts the longitudinal direction) of the transformed system, but the integral is still invariant. In defining $\psi' = \bar{g}\psi$ we are keeping the spin projection along the same, untransformed direction. Therefore the spin-polarization of the transformed system could in principle be related to that of the original system along any fixed projection direction, since the spin-resolved conductance satisfy a similar equation to (3):

$$G_{s',s}^{AB}(E) = \frac{e^2}{h} \sum_{i=1}^{M_A} \sum_{j=1}^{M_B} \left| \sum_{s_1, s_1'} \mathcal{D}^{1/2}(g)_{s',s_1'} \mathcal{D}^{1/2}(g)^*_{s,s_1} \int_{\mathbb{R}^3} \psi_{s_1'}^{\beta_j}(\mathbf{r})'^* \hat{S}(\mathbf{r})' \psi_{s_1}^{\alpha_i}(\mathbf{r})' d^3\mathbf{r} \right|^2, \quad \forall g \in O(3) \setminus \mathcal{G} \quad (13)$$

If the electrodes are fixed and the molecule is rotated around the longitudinal direction by an operation which is not a symmetry of the molecule (otherwise equation (5) would apply) or the electrodes (otherwise equation (13) would apply, since it would be equivalent to rotating the whole system), then the integral in equation (2) is not invariant under this transformation and the new components (in the rotated system, but along the original direction) of the spin-polarization are in general unrelated to the old ones, as can be observed in each subfigure of Figs. 3 and 4. The exception being if the rotation is geometrically equivalent to a longitudinal reflection, in which case equation (14) applies.

If a chiral molecule is placed between the electrodes, then the system cannot have planes of symmetry (more precisely and assuming that the molecule also lacks inversion symmetry, $\mathcal{G} \subset SO(3)$). It follows from equation (13) that the substitution, while keeping the electrodes fixed, of a chiral molecule by its enantiomeric partner may in principle yield a spin-polarization that is related to the original in a deterministic way (that is, independent on the symmetry-compatible details of the system). For equation (13) to be applicable, it is necessary that the system of electrodes possesses a symmetry plane, and to connect the molecule in such a way that the whole system is obtained from the original by reflection through that mirror plane, as done in Fig. 4. Two cases can then be distinguished, corresponding to the two essentially different ways to connect the enantiomer (both of them related by a π -rotation of the molecule around an axis perpendicular to the longitudinal direction, which swaps the anchoring to the electrodes), which we label by enant_1 , enant_2 :

- The system of electrodes has a longitudinal symmetry plane σ_l , containing the longitudinal direction. Let t_{\parallel}, t_{\perp} be transversal directions parallel and perpendicular, respectively, to σ_l . Then following the discussion of equation (5) and employing equation (13) with $g = \sigma_l$, we obtain:

$$\left\{ \begin{array}{l} \text{Longitudinal spin projection (} l \text{):} \\ \text{Transversal spin projection, parallel to } \sigma_l \text{ (} t_{\parallel} \text{):} \\ \text{Transversal spin projection, normal to } \sigma_l \text{ (} t_{\perp} \text{):} \end{array} \right. \begin{array}{l} G_{s',s}^{AB}(E) = G_{\bar{s},\bar{s}}^{AB}(E)^{\text{enant}_1} \Rightarrow P_l^{\text{enant}_1} = -P_l \\ G_{s',s}^{AB}(E) = G_{s',\bar{s}}^{AB}(E)^{\text{enant}_1} \Rightarrow P_{t_{\parallel}}^{\text{enant}_1} = -P_{t_{\parallel}} \\ G_{s',s}^{AB}(E) = G_{s',s}^{AB}(E)^{\text{enant}_1} \Rightarrow P_{t_{\perp}}^{\text{enant}_1} = P_{t_{\perp}} \end{array} \quad (14)$$

where $G_{s',s}^{AB}(E)^{\text{enant}_1} = \frac{e^2}{h} \sum_{i=1}^{M_A} \sum_{j=1}^{M_B} \left| \int_{\mathbb{R}^3} (\bar{\sigma}_l \psi_{s'_i}^{\beta_j}(\mathbf{r})^*) S(\sigma_l^{-1} \mathbf{r}) (\bar{\sigma}_l \psi_{s_j}^{\alpha_i}(\mathbf{r})) d^3 \mathbf{r} \right|^2$ is the conductance in the system with the present connection of the enantiomeric partner of the original molecule.

Usually there will be more than one such plane of symmetry for the system of electrodes, each of them determining a position of the enantiomer (all of them related by a rotation of the molecule alone around the longitudinal direction) for which the spin-polarization is related to that of the original molecule.

- The system of electrodes has a transversal symmetry plane σ_t , perpendicular to the longitudinal direction. This operation is uniquely determined in our configuration and it permutes the electrodes, so that following the discussion of equation (8) (in particular, invoking time reversal symmetry) and employing equation (13) with $g = \sigma_t$, we obtain:

$$\left\{ \begin{array}{l} \text{Longitudinal spin projection (} l \text{):} \\ \text{Transversal spin projection (} t \text{):} \end{array} \right. \begin{array}{l} G_{s',s}^{AB}(E) = G_{\bar{s},\bar{s}'}^{AB}(E)^{\text{enant}_2} \Rightarrow \text{No conclusive relation between } P_l, P_l^{\text{enant}_2} \\ G_{s',s}^{AB}(E) = G_{s',s'}^{AB}(E)^{\text{enant}_2} \Rightarrow \text{No conclusive relation between } P_t, P_t^{\text{enant}_2} \end{array} \quad (15)$$

where $G_{s',s}^{AB}(E)^{\text{enant}_2}$ is defined in analogy with $G_{s',s}^{AB}(E)^{\text{enant}_1}$, only changing σ_l by σ_t .

There is then one connection of the enantiomer, enant_2 , that may yield a spin-polarization which is unrelated, neither equal nor opposite, to that of the original molecule. This is no longer true if (and only if, in our configuration) the system of electrodes has both symmetries σ_l, σ_t and the original system, including the chiral molecule, has a transversal $C_{2,t_{\parallel}}$ rotation symmetry whose axis is parallel to the plane σ_t , so that $\sigma_t = \sigma_l C_{2,t_{\parallel}}$. In this case, successively applying equations (8), (14) in the right hand side, and equations (7), (15) in the left hand side ($\sigma_t \Theta = \sigma_l \Theta C_{2,t_{\parallel}}$), it follows that:

$$\left\{ \begin{array}{l} \text{Longitudinal spin projection (} l \text{):} \\ \text{Transversal spin projection, parallel to } \sigma_l \text{ and } C_2 \text{ (} t_{\parallel} \text{):} \\ \text{Transversal spin projection, normal to } \sigma_l \text{ and } C_2 \text{ (} t_{\perp} \text{):} \end{array} \right. \begin{array}{l} G_{\bar{s},\bar{s}'}^{AB}(E)^{\text{enant}_2} = G_{\bar{s},\bar{s}}^{AB}(E)^{\text{enant}_1} \Rightarrow P_l^{\text{enant}_2} = P_l^{\text{enant}_1} = -P_l \\ G_{s',s'}^{AB}(E)^{\text{enant}_2} = G_{s',s}^{AB}(E)^{\text{enant}_1} \Rightarrow P_{t_{\parallel}}^{\text{enant}_2} = P_{t_{\parallel}}^{\text{enant}_1} = -P_{t_{\parallel}} \\ G_{s',s'}^{AB}(E)^{\text{enant}_2} = G_{s',s}^{AB}(E)^{\text{enant}_1} \Rightarrow P_{t_{\perp}}^{\text{enant}_2} = P_{t_{\perp}}^{\text{enant}_1} = P_{t_{\perp}} \end{array} \quad (16)$$

which effectively makes the polarization equal for the two ways of connecting the enantiomer. This was to be expected, since both systems are identical due to the $C_{2,t_{\parallel}}$ symmetry.

Acknowledgements

J.J.P. and M.A.G.B acknowledge financial support from Spanish MICIN through Grant No. PID2019-109539GB-C43/AEI/10.13039/501100011033, the María de Maeztu Program for Units of Excellence in R&D (Grant No. CEX2018-000805-M), the Comunidad Autónoma de Madrid through the Nanomag COST-CM Program (Grant No. S2018/NMT-4321), the Generalitat Valenciana through Programa Prometeo/2021/01, the Centro de Computación Científica of the Universidad Autónoma de Madrid, and the computer resources of the Red Española de Supercomputación. L.A.Z. thanks financial support from MCIN/AEI/10.13039/501100011033 (grant PID2021-125604NB-I00) and from the Universidad Autónoma de Madrid/Comunidad de Madrid (grant No. SI3/PJI/2021-00191). S.P. acknowledges the grant from Erasmus+ 2018 programme (Collaboration between University of Tehran, Iran and Autonomous University of Madrid, Spain). W. D. thanks A. E. Botha for sharing python scripts used to make some of the figures in this work. The computational results contained in this work would also not have been possible without access to the high performance computing (HPC) facility at Unisa and the supercomputing facility in the Department of Applied Physics at the University of Alicante.

Author contributions

W.D and M.A.G.B contributed equally to this work, the former carrying out the DFT calculations and a basic theoretical analysis and the latter the full theoretical symmetry analysis. Both also contributed to the writing of the manuscript. L.Z.

brought to our attention the problem and carried out preliminary calculations. E.B.L. provided computational support, aided with guidance on presentation of numerical results and figures, discussions on the theoretical implications and contributed to the editing of the manuscript. S.P. provided the original code to implement SOC in ANT.Gaussian. C.S. aided with calculations and discussions on the experimental implications. J.J.P. had the original idea, coordinated the team, and contributed to the writing.

Competing interests

The authors declare no competing interests.

References

1. LaShell, S., McDougall, B. A. & Jensen, E. Spin splitting of an au(111) surface state band observed with angle resolved photoelectron spectroscopy. *Phys. Rev. Lett.* **77**, 3419–3422, DOI: [10.1103/PhysRevLett.77.3419](https://doi.org/10.1103/PhysRevLett.77.3419) (1996).
2. Hoesch, M. *et al.* Spin structure of the shockley surface state on Au(111). *Phys. Rev. B* **69**, 241401, DOI: [10.1103/PhysRevB.69.241401](https://doi.org/10.1103/PhysRevB.69.241401) (2004).
3. Qi, X.-L. & Zhang, S.-C. Topological insulators and superconductors. *Rev. Mod. Phys.* **83**, 1057–1110, DOI: [10.1103/RevModPhys.83.1057](https://doi.org/10.1103/RevModPhys.83.1057) (2011).
4. Wunderlich, J., Kaestner, B., Sinova, J. & Jungwirth, T. Experimental observation of the spin-hall effect in a two-dimensional spin-orbit coupled semiconductor system. *Phys. Rev. Lett.* **94**, 047204, DOI: [10.1103/PhysRevLett.94.047204](https://doi.org/10.1103/PhysRevLett.94.047204) (2005).
5. Kato, Y. K., Myers, R. C., Gossard, A. C. & Awschalom, D. D. Observation of the spin hall effect in semiconductors. *Science* **306**, 1910–1913, DOI: [10.1126/science.1105514](https://doi.org/10.1126/science.1105514) (2004). <https://www.science.org/doi/pdf/10.1126/science.1105514>.
6. Safeer, C. K. *et al.* Large multidirectional spin-to-charge conversion in low-symmetry semimetal mote2 at room temperature. *Nano Lett.* **19**, 8758–8766, DOI: [10.1021/acs.nanolett.9b03485](https://doi.org/10.1021/acs.nanolett.9b03485) (2019). <https://doi.org/10.1021/acs.nanolett.9b03485>.
7. Rassekh, M. *et al.* Charge-spin interconversion in graphene-based systems from density functional theory. *Phys. Rev. B* **104**, 1–9, DOI: [10.1103/PhysRevB.104.235429](https://doi.org/10.1103/PhysRevB.104.235429) (2021).
8. Ingla-Aynés, J. *et al.* Omnidirectional spin-to-charge conversion in graphene/nbse2 van der waals heterostructures. *2D Mater.* **9**, 045001, DOI: [10.1088/2053-1583/ac76d1](https://doi.org/10.1088/2053-1583/ac76d1) (2022).
9. Benítez, L. A. *et al.* Tunable room-temperature spin galvanic and spin hall effects in van der waals heterostructures. *Nat. Mater.* **19**, 170–175 (2020).
10. Calavalle, F. *et al.* Gate-tuneable and chirality-dependent charge-to-spin conversion in tellurium nanowires. *Nat. Mater.* **21**, 526–532, DOI: [10.1038/s41563-022-01211-7](https://doi.org/10.1038/s41563-022-01211-7) (2022).
11. D'Yakonov, M. I. & Perel', V. I. Possibility of Orienting Electron Spins with Current. *Sov. J. Exp. Theor. Phys. Lett.* **13**, 467 (1971).
12. Sinova, J. *et al.* Universal intrinsic spin hall effect. *Phys. Rev. Lett.* **92**, 126603, DOI: [10.1103/PhysRevLett.92.126603](https://doi.org/10.1103/PhysRevLett.92.126603) (2004).
13. Valenzuela, S. O. & Tinkham, M. Direct electronic measurement of the spin hall effect. *Nature* **442**, 176–179, DOI: [10.1038/nature04937](https://doi.org/10.1038/nature04937) (2006).
14. Edelstein, V. Spin polarization of conduction electrons induced by electric current in two-dimensional asymmetric electron systems. *Solid State Commun.* **73**, 233–235, DOI: [https://doi.org/10.1016/0038-1098\(90\)90963-C](https://doi.org/10.1016/0038-1098(90)90963-C) (1990).
15. Zhai, F. & Xu, H. Symmetry of spin transport in two-terminal waveguides with a spin-orbital interaction and magnetic field modulations. *Phys. review letters* **94**, 246601 (2005).
16. Nikolić, B. K. & Souma, S. Decoherence of transported spin in multichannel spin-orbit-coupled spintronic devices: Scattering approach to spin-density matrix from the ballistic to the localized regime. *Phys. Rev. B* **71**, 195328 (2005).
17. Pareek, T. P. Pure spin currents and the associated electrical voltage. *Phys. Rev. Lett.* **92**, 076601, DOI: [10.1103/PhysRevLett.92.076601](https://doi.org/10.1103/PhysRevLett.92.076601) (2004).
18. Gmitra, M., Konschuh, S., Ertler, C., Ambrosch-Draxl, C. & Fabian, J. Band-structure topologies of graphene: Spin-orbit coupling effects from first principles. *Phys. Rev. B* **80**, 235431, DOI: [10.1103/PhysRevB.80.235431](https://doi.org/10.1103/PhysRevB.80.235431) (2009).
19. Gmitra, M., Kochan, D., Högl, P. & Fabian, J. Trivial and inverted dirac bands and the emergence of quantum spin hall states in graphene on transition-metal dichalcogenides. *Phys. Rev. B* **93**, 155104 (2016).

20. Ray, K., Ananthavel, S. P., Waldeck, D. H. & Naaman, R. Asymmetric scattering of polarized electrons by organized organic films of chiral molecules. *Science* **283**, 814–816, DOI: [10.1126/science.283.5403.814](https://doi.org/10.1126/science.283.5403.814) (1999). <https://www.science.org/doi/pdf/10.1126/science.283.5403.814>.
21. Xie, Z. *et al.* Spin specific electron conduction through dna oligomers. *Nano Lett.* **11**, 4652–4655, DOI: [10.1021/nl2021637](https://doi.org/10.1021/nl2021637) (2011). <https://doi.org/10.1021/nl2021637>.
22. Dor, O. B., Yochelis, S., Mathew, S. P., Naaman, R. & Paltiel, Y. A chiral-based magnetic memory device without a permanent magnet. *Nat. Commun.* **4**, 2256, DOI: [10.1038/ncomms3256](https://doi.org/10.1038/ncomms3256) (2013).
23. Mondal, P. C. *et al.* Chiral Conductive Polymers as Spin Filters. *Adv. Mater.* **27**, 1924–1927, DOI: [10.1002/adma.201405249](https://doi.org/10.1002/adma.201405249) (2015).
24. Kiran, V. *et al.* Helicenes - A New Class of Organic Spin Filter. *Adv. Mater.* **28**, 1957–1962, DOI: [10.1002/adma.201504725](https://doi.org/10.1002/adma.201504725) (2016).
25. Aragonès, A. C. *et al.* Measuring the Spin-Polarization Power of a Single Chiral Molecule. *Small* **13**, 1–6, DOI: [10.1002/sml.201602519](https://doi.org/10.1002/sml.201602519) (2017).
26. Ghosh, S., Bloom, B. P., Lu, Y., Lamont, D. & Waldeck, D. H. Increasing the efficiency of water splitting through spin polarization using cobalt oxide thin film catalysts. *The J. Phys. Chem. C* **124**, 22610–22618, DOI: [10.1021/acs.jpcc.0c07372](https://doi.org/10.1021/acs.jpcc.0c07372) (2020). <https://doi.org/10.1021/acs.jpcc.0c07372>.
27. Liu, T. *et al.* Linear and nonlinear two-terminal spin-valve effect from chirality-induced spin selectivity. *ACS Nano* **14**, 15983–15991, DOI: [10.1021/acsnano.0c07438](https://doi.org/10.1021/acsnano.0c07438) (2020). <https://doi.org/10.1021/acsnano.0c07438>.
28. Mondal, A. K. *et al.* Spin filtering in supramolecular polymers assembled from achiral monomers mediated by chiral solvents. *J. Am. Chem. Soc.* **143**, 7189–7195, DOI: [10.1021/jacs.1c02983](https://doi.org/10.1021/jacs.1c02983) (2021). <https://doi.org/10.1021/jacs.1c02983>.
29. Wei, M. *et al.* Response of spin to chiral orbit and phonon in organic chiral ferrimagnetic crystals. *ACS Nano* **16**, 13049–13056, DOI: [10.1021/acsnano.2c05601](https://doi.org/10.1021/acsnano.2c05601) (2022). <https://doi.org/10.1021/acsnano.2c05601>.
30. Adhikari, Y. *et al.* Interplay of structural chirality, electron spin and topological orbital in chiral molecular spin valves, DOI: [10.48550/ARXIV.2209.08117](https://doi.org/10.48550/ARXIV.2209.08117) (2022).
31. Naaman, R., Paltiel, Y. & Waldeck, D. H. Chiral molecules and the spin selectivity effect. *The J. Phys. Chem. Lett.* **11**, 3660–3666 (2020).
32. Naaman, R. & Waldeck, D. H. Chiral-Induced Spin Selectivity Effect. *J. Phys. Chem. C* **3**, 2178–2187, DOI: [10.1021/jz300793y](https://doi.org/10.1021/jz300793y) (2012).
33. Gutierrez, R. *et al.* Modeling spin transport in helical fields: Derivation of an effective low-dimensional hamiltonian. *J. Phys. Chem. C* **117**, 22276–22284, DOI: [10.1021/jp401705x](https://doi.org/10.1021/jp401705x) (2013).
34. Gersten, J., Kaasbjerg, K. & Nitzan, A. Induced spin filtering in electron transmission through chiral molecular layers adsorbed on metals with strong spin-orbit coupling. *J. Chem. Phys.* **139**, 114111, DOI: [10.1063/1.4820907](https://doi.org/10.1063/1.4820907) (2013).
35. Naaman, R., Paltiel, Y. & Waldeck, D. H. Chiral molecules and the electron spin. *Nat. Rev. Chem.* **3**, 250–260, DOI: [10.1038/s41570-019-0087-1](https://doi.org/10.1038/s41570-019-0087-1) (2019).
36. Dalum, S. & Hedegård, P. Theory of Chiral Induced Spin Selectivity. *Nano Lett.* **19**, 5253–5259, DOI: [10.1021/acs.nanolett.9b01707](https://doi.org/10.1021/acs.nanolett.9b01707) (2019).
37. Yang, X., van der Wal, C. H. & van Wees, B. J. Spin-dependent electron transmission model for chiral molecules in mesoscopic devices. *Phys. Rev. B* **99**, 024418 (2019).
38. Yang, X., van der Wal, C. H. & van Wees, B. J. Detecting chirality in two-terminal electronic nanodevices. *Nano letters* **20**, 6148–6154 (2020).
39. Zöllner, M. S., Varela, S., Medina, E., Mujica, V. & Herrmann, C. Insight into the origin of chiral-induced spin selectivity from a symmetry analysis of electronic transmission. *J. Chem. Theory Comput.* **16**, 2914–2929, DOI: [10.1021/acs.jctc.9b01078](https://doi.org/10.1021/acs.jctc.9b01078) (2020).
40. Zöllner, M. S., Saghatchi, A., Mujica, V. & Herrmann, C. Influence of electronic structure modeling and junction structure on first-principles chiral induced spin selectivity. *J. Chem. Theory Comput.* **16**, 7357–7371, DOI: [10.1021/acs.jctc.0c00621](https://doi.org/10.1021/acs.jctc.0c00621) (2020).
41. Alwan, S. & Dubi, Y. Spinterface origin for the chirality-induced spin-selectivity effect. *J. Am. Chem. Soc.* **143**, 14235–14241 (2021).

42. Liu, Y., Xiao, J., Koo, J. & Yan, B. Chirality-driven topological electronic structure of DNA-like materials. *Nat. Mater.* **20**, 638–644, DOI: [10.1038/s41563-021-00924-5](https://doi.org/10.1038/s41563-021-00924-5) (2021).
43. Fransson, J. Charge and spin dynamics and enantioselectivity in chiral molecules. *The J. Phys. Chem. Lett.* **13**, 808–814, DOI: [10.1021/acs.jpcclett.1c03925](https://doi.org/10.1021/acs.jpcclett.1c03925) (2022). <https://doi.org/10.1021/acs.jpcclett.1c03925>.
44. Dubi, Y. Spinterface chirality-induced spin selectivity effect in bio-molecules. *Chem. science* **13**, 10878–10883 (2022).
45. Evers, F. *et al.* Theory of chirality induced spin selectivity: Progress and challenges. *Adv. Mater.* **34**, 2106629, DOI: <https://doi.org/10.1002/adma.202106629> (2022). <https://onlinelibrary.wiley.com/doi/pdf/10.1002/adma.202106629>.
46. Wolf, Y., Liu, Y., Xiao, J., Park, N. & Yan, B. Unusual spin polarization in the chirality-induced spin selectivity. *ACS Nano* **0**, null, DOI: [10.1021/acsnano.2c07088](https://doi.org/10.1021/acsnano.2c07088) (2022). <https://doi.org/10.1021/acsnano.2c07088>.
47. Fransson, J. Chirality-induced spin selectivity: The role of electron correlations. *The J. Phys. Chem. Lett.* **10**, 7126–7132, DOI: [10.1021/acs.jpcclett.9b02929](https://doi.org/10.1021/acs.jpcclett.9b02929) (2019). <https://doi.org/10.1021/acs.jpcclett.9b02929>.
48. Du, G.-F., Fu, H.-H. & Wu, R. Vibration-enhanced spin-selective transport of electrons in the dna double helix. *Phys. Rev. B* **102**, 035431, DOI: [10.1103/PhysRevB.102.035431](https://doi.org/10.1103/PhysRevB.102.035431) (2020).
49. Fransson, J. Vibrational origin of exchange splitting and "chiral-induced spin selectivity. *Phys. Rev. B* **102**, 235416, DOI: [10.1103/PhysRevB.102.235416](https://doi.org/10.1103/PhysRevB.102.235416) (2020).
50. Zhang, L., Hao, Y., Qin, W., Xie, S. & Qu, F. Chiral-induced spin selectivity: A polaron transport model. *Phys. Rev. B* **102**, 214303, DOI: [10.1103/PhysRevB.102.214303](https://doi.org/10.1103/PhysRevB.102.214303) (2020).
51. Teh, H.-H., Dou, W. & Subotnik, J. E. Antisymmetric berry frictional force at equilibrium in the presence of spin-orbit coupling. *Phys. Rev. B* **104**, L201409, DOI: [10.1103/PhysRevB.104.L201409](https://doi.org/10.1103/PhysRevB.104.L201409) (2021).
52. Fransson, J. Charge redistribution and spin polarization driven by correlation induced electron exchange in chiral molecules. *Nano Lett.* **21**, 3026–3032, DOI: [10.1021/acs.nanolett.1c00183](https://doi.org/10.1021/acs.nanolett.1c00183) (2021). <https://doi.org/10.1021/acs.nanolett.1c00183>.
53. Fransson, J. The chiral induced spin selectivity effect – what it is, what it is not, and why it matters, DOI: [10.48550/ARXIV.2202.02512](https://doi.org/10.48550/ARXIV.2202.02512) (2022).
54. Chico, L., Latgé, A. & Brey, L. Symmetries of quantum transport with Rashba spin-orbit: graphene spintronics. *Phys. Chem. Chem. Phys.* **17**, 16469–16475, DOI: [10.1039/c5cp01637a](https://doi.org/10.1039/c5cp01637a) (2015). [1503.04154](https://doi.org/10.1039/c5cp01637a).
55. Guo, A. M., Pan, T. R., Fang, T. F., Xie, X. C. & Sun, Q. F. Spin selectivity effect in achiral molecular systems. *Phys. Rev. B* **94**, 1–5, DOI: [10.1103/PhysRevB.94.165409](https://doi.org/10.1103/PhysRevB.94.165409) (2016).
56. Sabater, C., Untiedt, C., Palacios, J. J. & Caturla, M. J. Mechanical annealing of metallic electrodes at the atomic scale. *Phys. Rev. Lett.* **108**, 205502, DOI: [10.1103/PhysRevLett.108.205502](https://doi.org/10.1103/PhysRevLett.108.205502) (2012).
57. Palacios, J. J., Pérez-Jiménez, A. J., Louis, E. & Vergés, J. A. Fullerene-based molecular nanobridges: A first-principles study. *Phys. Rev. B* **64**, 115411, DOI: [10.1103/PhysRevB.64.115411](https://doi.org/10.1103/PhysRevB.64.115411) (2001).
58. Palacios, J. J., Pérez-Jiménez, A. J., Louis, E., SanFabián, E. & Vergés, J. A. First-principles approach to electrical transport in atomic-scale nanostructures. *Phys. Rev. B* **66**, 035322, DOI: [10.1103/PhysRevB.66.035322](https://doi.org/10.1103/PhysRevB.66.035322) (2002).
59. Louis, E., Vergés, J. A., Palacios, J. J., Pérez-Jiménez, A. J. & SanFabián, E. Implementing the keldysh formalism into ab initio methods for the calculation of quantum transport: Application to metallic nanocontacts. *Phys. Rev. B* **67**, 155321, DOI: [10.1103/PhysRevB.67.155321](https://doi.org/10.1103/PhysRevB.67.155321) (2003).
60. Palacios, J. J. *et al.* Computer code ANT.Gaussian, with SOC corrections. Available from <https://github.com/juanjosepalacios/ANT.Gaussian>.
61. Fernández-Rossier, J. & Palacios, J. J. Magnetism in graphene nanoislands. *Phys. Rev. Lett.* **99**, 177204, DOI: [10.1103/PhysRevLett.99.177204](https://doi.org/10.1103/PhysRevLett.99.177204) (2007).
62. Kulkarni, C. *et al.* Highly efficient and tunable filtering of electrons' spin by supramolecular chirality of nanofiber-based materials. *Adv. Mater.* **32**, 1904965, DOI: <https://doi.org/10.1002/adma.201904965> (2020). <https://onlinelibrary.wiley.com/doi/pdf/10.1002/adma.201904965>.
63. Fisher, D. S. & Lee, P. A. Relation between conductivity and transmission matrix. *Phys. Rev. B* **23**, 6851 (1981).
64. Chico, L., Benedict, L. X., Louie, S. G. & Cohen, M. L. Quantum conductance of carbon nanotubes with defects. *Phys. Rev. B* **54**, 2600 (1996).
65. Datta, S. *Electronic transport in mesoscopic systems* (Cambridge university press, 1997).

66. Chen, X., Xu, Y., Wang, J. & Guo, H. Valley filtering effect of phonons in graphene with a grain boundary. *Phys. Rev. B* **99**, 064302 (2019).
67. Beenakker, C. W. Random-matrix theory of quantum transport. *Rev. modern physics* **69**, 731 (1997).
68. Utsumi, Y., Entin-Wohlman, O. & Aharony, A. Spin selectivity through time-reversal symmetric helical junctions. *Phys. Rev. B* **102**, 035445 (2020).
69. Merzbacher, E. *Quantum mechanics* (John Wiley & Sons, 1998).
70. Belkić, D. *Principles of quantum scattering theory* (CRC Press, 2020).
71. Bir, G. L. & Pikus, G. E. *Symmetry and strain-induced effects in semiconductors* (Wiley New York, 1974).
72. Schnyder, A. P., Ryu, S., Furusaki, A. & Ludwig, A. W. Classification of topological insulators and superconductors in three spatial dimensions. *Phys. Rev. B* **78**, 195125 (2008).

SUPPLEMENTARY INFORMATION: A group-theoretic approach to the origin of chirality-induced spin selectivity in non-magnetic molecular junctions

W. Dednam^{1,*}, M. A. García-Blázquez^{2,*}, Linda A. Zotti^{3,4}, E. B. Lombardi¹, C. Sabater⁵, S. Pakdel⁶, and J. J. Palacios^{2,7} ✉

- ¹ Department of Physics, Florida Science Campus, University of South Africa, 1710 Johannesburg, South Africa
² Departamento de Física de la Materia Condensada, Universidad Autónoma de Madrid, E-28049 Madrid, Spain
³ Departamento de Física Teórica de la Materia Condensada, Universidad Autónoma de Madrid, E-28049 Madrid, Spain
⁴ Condensed Matter Physics Center (IFIMAC), Universidad Autónoma de Madrid, E-28049 Madrid, Spain
⁵ Departamento de Física Aplicada and Unidad asociada CSIC, Universidad de Alicante, E-03690 Alicante, Spain
⁶ CAMD, Department of Physics, Technical University of Denmark, 2800 Kgs. Lyngby, Denmark
⁷ Instituto Nicolás Cabrera (INC) and Condensed Matter Physics Center (IFIMAC), Universidad Autónoma de Madrid, E-28049 Madrid, Spain

* These authors contributed equally to this work

✉ e-mail: juanjose.palacios@uam.es

ABSTRACT

Quantum transport calculations described in this *SI* and based on density functional theory corroborate each one of our predictions in the main manuscript and offer us further quantitative insight.

1 SOC-corrected DFT transport calculations

Pakdel et al.¹ developed a convenient method to correct the band structure of solid materials for spin-orbit coupling (SOC). The core feature of this approach is that quality SOC-corrected bands can be obtained if an existing (or optimized) Gaussian-type orbital (GTO) basis set already reproduces the non-SOC band structure of a material to a good degree, so that SOC can be treated perturbatively. Once that condition is met, adding SOC as a correction in a post self-consistent-field (SCF) step gives good bands in comparison to reference methods which are known to generate very high quality SOC bands by fully-relativistic self-consistent approaches, e.g., VASP², Wien2k³, Quantum Espresso⁴ or OpenMX⁵⁻⁸. The latter is used as the reference method in this work.

Here we very briefly outline the method developed by Pakdel et al.¹ in addition to a few recent improvements we have made to it. We use the standard atomic SOC matrix to express the lowest-order Dirac-Kohn-Sham Hamiltonian as follows:

$$\xi(r) \mathbf{L} \cdot \mathbf{S} = \left[\xi_{ij} \langle l_i; m_i; s | \mathbf{L} \cdot \mathbf{S} | l_j; m_j; s' \rangle \right], \quad (1)$$

where:

$$\xi_{ij} = \frac{e^2}{2m_e c^2} \int_0^\infty \frac{1}{r} \frac{dV_{\text{eff}}(r)}{dr} R_i(r) R_j^*(r) r^2 dr. \quad (2)$$

The above simplification relies upon the orthogonality of the radial and angular parts of wave functions in atomic-orbital based DFT, e.g., the Gaussian-type orbitals (GTOs) used by CRYSTAL14⁹ or GAUSSIAN09¹⁰.

The effective nuclear potential in Eq. (2) is defined as $V_{\text{eff}}(r) = -\frac{Z}{r}$, with Z the atomic number. The radial wave functions $R_i(r)$ are (un)contracted GTOs (CGTOs). The fact that SOC is an intra-atomic phenomenon means that only CGTOs on the same atom and of the same shell type ($L = 1, 2$ or 3 , referring to P, D , or F shells, respectively) contribute to the integral in Eq. (2)¹. Note that, due to the lack of adequate nodal structure near the nucleus in pseudopotentials, CGTO basis sets with pseudopotentials require a multiplicative correction to ξ_{ij} if $V_{\text{eff}}(r)$ is to reproduce the correct effective charge of a given atom.

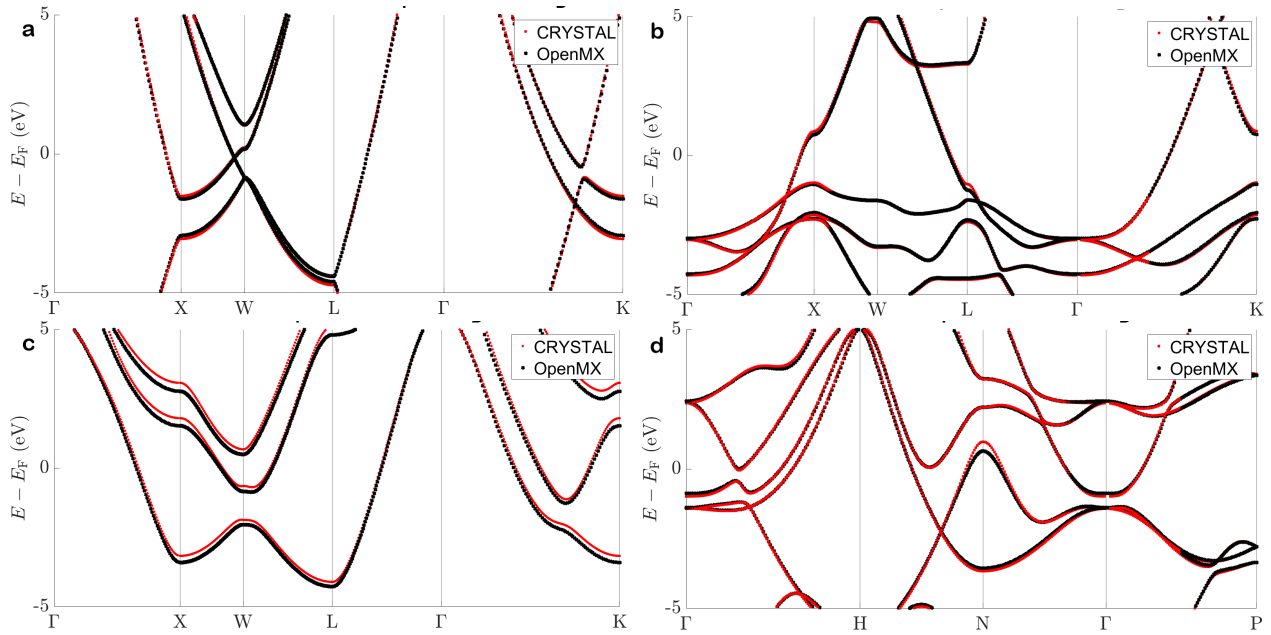


Figure 1. SOC-corrected bands obtained from previous non-SOC calculations in CRYSTAL14 using our method (solid red markers) and the reference method OpenMX (black crosses) for FCC **a** Al, **b** Au, **c** Pb and **d** BCC W.

We describe two minor modifications that improve upon the method described in Ref.¹. First, we have replaced the original effective nuclear potential by a Yukawa screening potential:

$$V_{\text{eff}}(r) = \begin{cases} \frac{-(Z-1)[\exp(-\frac{\ln Z}{r_c}r)+1]}{r} & r \leq r_c \\ \frac{-1}{r} & r > r_c \end{cases} \quad (3)$$

where r_c is a cutoff, typically the size of an atomic radius ($\sim 2.5 - 3.0$ a.u.).

Secondly, we do not use a single global multiplicative factor to account for the lack of nodal structure when basis sets with pseudopotentials are used. Instead, we have implemented a multiplicative factor for each shell type (P , D , or F) because it is known that the radial SOC coefficients of different angular momentum shells are multiples of each other¹¹.

The ultimate goal of fitting SOC corrected bands to a reference method is to choose high quality basis sets that can be used in DFT quantum transport calculations where transition metal elements, sometimes with strong SOC, are used as the electrodes. We therefore need such GTO basis sets for metals like Al, Au, Pb, and W, which are used as electrode and/or substrate materials in scanning tunneling microscopy (STM) or mechanically controllable break junction (MCBJ) experiments¹²⁻¹⁴. In this work, the basis sets used in our electronic transport calculations in the main manuscript have also been employed in band structure calculations in CRYSTAL14 to make Fig. 1, which shows an empirical fit of SOC-corrected bands to OpenMX band structure calculations for Al, Au, Pb and W. For an all-electron basis set, the multiplicative factors (P , D , or F) per shell should all be 1 as in the calculation for FCC Al shown in Fig. 1a in which we used a high quality all-electron basis set which has been optimized for the metal phase of Al¹⁵. (For Au and W we used basis sets from Ref.¹⁶ and for Pb we used the basis set from¹⁷. All basis sets required optimization of their outer diffuse GTOs in order to get the best empirical agreement with the reference method. We used the `billy` optimizer developed by Mike Towler for this purpose¹⁸.)

The implementation of SOC in our DFT electronic transport method is discussed in detail in other works¹⁹⁻²¹. We merely mention here that the code Atomistic NanoTransport (`ANT.Gaussian`)²²⁻²⁴, interfacing with `Gaussian09`¹⁰, has been employed in this work. Out of the box, it allows performing scalar-relativistic, spin-unrestricted calculations. The SOC correction as implemented in `ANT.Gaussian` is freely available online²⁵.

At this point, we believe it pertinent to mention that the small polarizations obtained across a wide energy range about the Fermi level in Ref.²⁶ in their Au-molecule-Au calculations using an all-electron basis set such as `x2c-SVPA11-2c`, if not optimized for the solid phase of the pure metal, may be the result of SOC not having any real effect on the electronic structure of the metal nanofragments that are used as electrodes. Figure 2 shows the bands without SOC in **a** and with SOC in **b** obtained from CRYSTAL14 calculations using the unoptimized all-electron basis set `x2c-SVPA11-2c`.

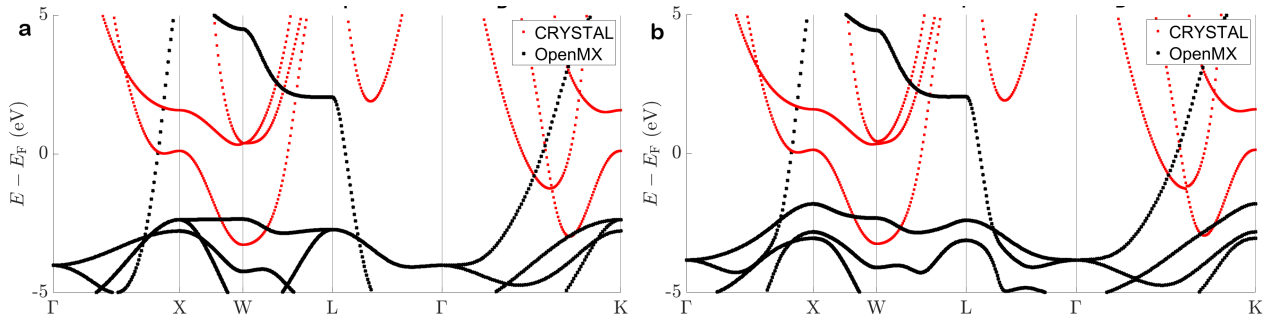


Figure 2. **a** Non-SOC and **b** SOC-corrected bands obtained in CRYSTAL14 calculations using the unoptimized $\times 2c-SVP_{all-2c}$ all-electron basis set for FCC Au in our method (solid red markers) and a large pseudo-potential basis set in the reference method OpenMX (black crosses). The fit is very poor and the addition of SOC does not seem to affect the electronic structure about the Fermi level in our method while the reference method clearly exhibits the lifting of degeneracies expected for a strong SOC metal such as Au and reproduced by our method too in Fig. 1. The reference bands in **b** differ slightly from those of Fig. 1b because a larger lattice parameter was required to converge the calculation using the all-electron basis set.

Finally, we obtain large polarization values even though reciprocity relations *a priori* prohibit spin-polarization in two-terminal devices in the coherent transport limit²⁷. However, in our calculations there are multiple “contact points” at the two interfaces between molecule and the finite-width electrodes due to tunneling and/or hopping. This means we can observe non-zero polarization in two-terminal coherent transport even in the absence of dephasing²⁸.

2 Results not included in the main text

Here we present the full polarization results, over a range of energies centred on the Fermi level, and corresponding to Fig. 2 of the main text. Figure 3 shows the zero-bias spin-polarization along the direction of transport as a function of energy at various angles of relative rotation for **a** Al(001), **b** Al(111), **c** Au(001), **d** Au(111), **e** W(001), **f** W(-110), **g** Pb(001) and **h** Pb(111) nanocontacts.

In Figs. 3a, 3b, as expected, Al always exhibits negligible polarization because SOC is very weak in this metal, while in Figs. 3c, d, one observes that Au exhibits the greatest spin-polarization well below the Fermi level. It also appears that W may exhibit non-negligible polarization at low bias voltage in experiments, as shown in Figs. 3e, f. Furthermore, Pb exhibits smaller polarization than Au, but over a larger range about the Fermi level. Also like Au, the Pb(001) nanocontacts exhibits larger polarization than the Pb(111) ones.

Finally, we explicitly show in Fig. 4 that when both longitudinal mirror and rotation symmetries are present in a structure the polarization is vanishing even when the quantization axis is neither parallel nor perpendicular to the direction of propagation (see blue line and inset in blue box in Fig. 4), which corresponds to a neither longitudinal nor transversal spin-polarization component. However, when the drain electrode is rotated 15° relative to the source electrode as in the red and green inset boxes, the longitudinal mirror is absent and only rotational symmetry remains, which as we saw in Fig. 2a of the main text does not force the polarization to vanish if the spin quantization axis has a projection along the current. The magnitude of the polarization (red) in the structure tilted at 45° with respect to the vertical quantization axis along \hat{z} is reduced relative to the structure oriented along \hat{z} .

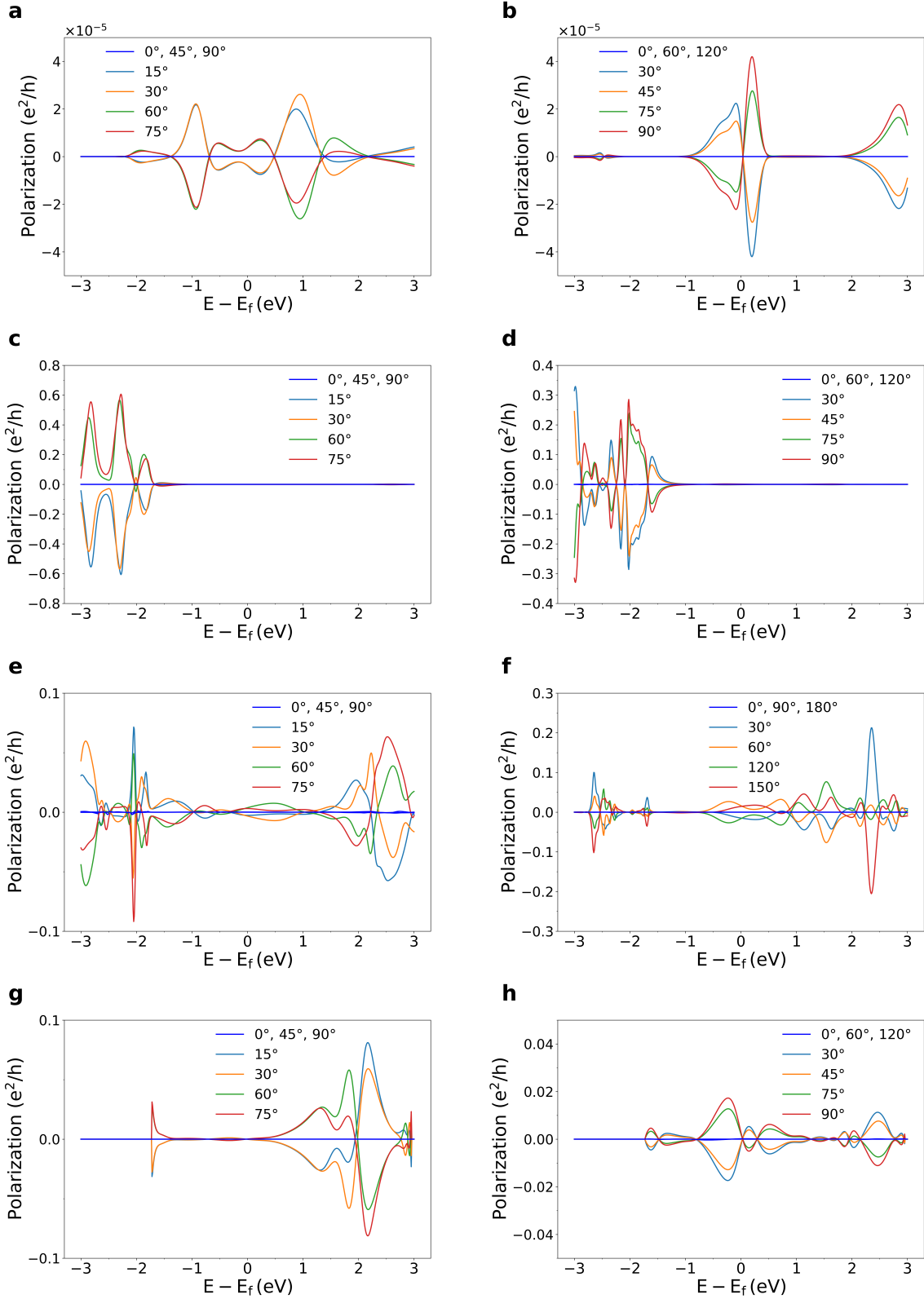


Figure 3. DFT-computed zero-bias spin-polarization along the direction of transport as a function of energy, for several angles of relative rotation between the electrodes (only the top half is rotated). **a**, Al(001). **b**, Al(111). **c**, Au(001). **d**, Au(111). **e**, W(001). **f**, W(-110). **g**, Pb(001). **h**, Pb(111) stacked nanocontacts.

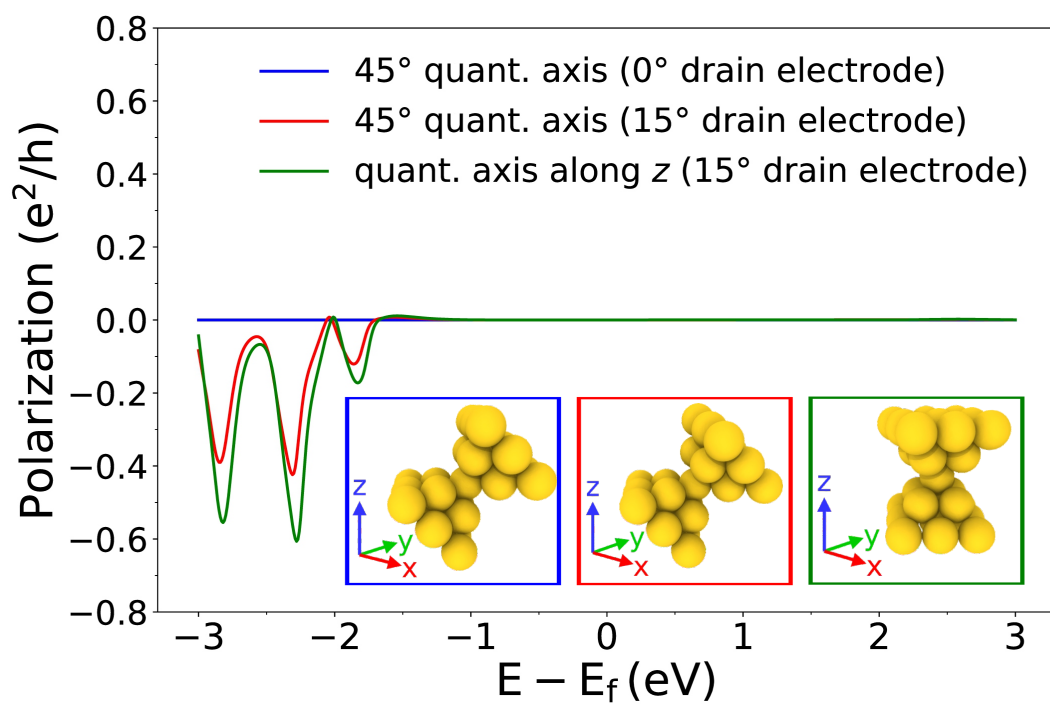


Figure 4. DFT-computed zero-bias spin-polarization along \hat{z} as a function of energy, for Au(001) nanocontacts. The 15° angles in the red and green inset boxes are obtained by rotating the drain electrode with respect to the source electrode.

References

1. Pakdel, S., Pourfath, M. & Palacios, J. J. An implementation of spin-orbit coupling for band structure calculations with gaussian basis sets: Two-dimensional topological crystals of sb and bi. *Beilstein J. Nanotechnol.* **9**, 1015 (2018).
2. Kresse, G. & Furthmüller, J. Efficiency of ab-initio total energy calculations for metals and semiconductors using a plane-wave basis set. *Comput. Mater. Sci.* **6**, 15–50, DOI: [https://doi.org/10.1016/0927-0256\(96\)00008-0](https://doi.org/10.1016/0927-0256(96)00008-0) (1996).
3. Blaha, P., Schwarz, K., Madsen, G., Kvasnicka, D. & Luitz, J. *Wien2k: An augmented plane wave+ local orbitals program for calculating crystal properties* (Karlheinz Schwarz, Techn. Universität Wien, Austria, 2001).
4. Giannozzi, P. *et al.* Quantum espresso: a modular and open-source software project for quantum simulations of materials. *J. Phys.: Condens. Matter* **21**, 395502 (2009).
5. Ozaki, T. Variationally optimized atomic orbitals for large-scale electronic structures. *Phys. Rev. B* **67**, 155108, DOI: [10.1103/PhysRevB.67.155108](https://doi.org/10.1103/PhysRevB.67.155108) (2003).
6. Ozaki, T. & Kino, H. Numerical atomic basis orbitals from h to kr. *Phys. Rev. B* **69**, 195113, DOI: [10.1103/PhysRevB.69.195113](https://doi.org/10.1103/PhysRevB.69.195113) (2004).
7. Ozaki, T. & Kino, H. Efficient projector expansion for the ab initio lcao method. *Phys. Rev. B* **72**, 045121, DOI: [10.1103/PhysRevB.72.045121](https://doi.org/10.1103/PhysRevB.72.045121) (2005).
8. Ozaki, T. *et al.* OpenMX (Open source package for Material eXplorer) ver. 3.8 (2017).
9. Dovesi, R. *et al.* Crystal14: A program for the ab initio investigation of crystalline solids. *Int. J. Quantum Chem.* **114**, 1287, DOI: [10.1002/qua.24658](https://doi.org/10.1002/qua.24658) (2014).
10. Frisch, M. J. *et al.* Computer code GAUSSIAN09, Revision C.01, Gaussian, Inc. Wallingford, CT, 2009.
11. Barreteau, C., Spanjaard, D. & Desjonquères, M.-C. An efficient magnetic tight-binding method for transition metals and alloys. *Comptes Rendus Physique* **17**, 406 (2016).
12. Agraït, N., Yeyati, A. L. & Van Ruitenbeek, J. M. Quantum properties of atomic-sized conductors. *Phys. Reports* **377**, 81 (2003).
13. Sabater, C. *et al.* Role of first-neighbor geometry in the electronic and mechanical properties of atomic contacts. *Phys. Rev. B* **97**, 075418 (2018).
14. Calvo, M. R. *et al.* Influence of relativistic effects on the contact formation of transition metals. *Phys. Rev. Lett.* **120**, 076802, DOI: [10.1103/PhysRevLett.120.076802](https://doi.org/10.1103/PhysRevLett.120.076802) (2018).
15. Ruiz, E., Llunell, M. & Alemany, P. Calculation of exchange coupling constants in solid state transition metal compounds using localized atomic orbital basis sets. *J. Solid State Chem.* **176**, 400–411, DOI: [https://doi.org/10.1016/S0022-4596\(03\)00238-X](https://doi.org/10.1016/S0022-4596(03)00238-X) (2003).
16. Laun, J. & Bredow, T. Bsse-corrected consistent gaussian basis sets of triple-zeta valence with polarization quality of the sixth period for solid-state calculations. *J. Comput. Chem.* **42**, 1064–1072, DOI: <https://doi.org/10.1002/jcc.26521> (2021).
17. Zagorac, D., Doll, K., Schön, J. C. & Jansen, M. Ab initio structure prediction for lead sulfide at standard and elevated pressures. *Phys. Rev. B - Condens. Matter Mater. Phys.* **84**, 1–13, DOI: [10.1103/PhysRevB.84.045206](https://doi.org/10.1103/PhysRevB.84.045206) (2011).
18. Towler, M. Computer code `billy` for optimizing CRYSTAL14 basis sets. Available from https://vallico.net/mike_towler/crystal.html.
19. Dednam, W. *Atomistic simulations of competing influences on electron transport across metal nanocontacts*. Ph.D. thesis, University of Alicante/University of South Africa (2019).
20. Dednam, W. *et al.* Refined electron-spin transport model for single-element ferromagnetic systems: Application to nickel nanocontacts. *Phys. Rev. B* **102**, 245415, DOI: [10.1103/PhysRevB.102.245415](https://doi.org/10.1103/PhysRevB.102.245415) (2020).
21. Dednam, W., Zotti, L. A., Pakdel, S., Lombardi, E. & Palacios, J. Spin-imbalances in non-magnetic nano-systems: Using non-equilibrium green's function dft to model spin-selective phenomena mediated by spin-orbit coupling. *Proc. 65th Annu. Conf. South Afr. Inst. Phys.* **65**, 25–30 (2022).
22. Palacios, J. J., Pérez-Jiménez, A. J., Louis, E. & Vergés, J. A. Fullerene-based molecular nanobridges: A first-principles study. *Phys. Rev. B* **64**, 115411, DOI: [10.1103/PhysRevB.64.115411](https://doi.org/10.1103/PhysRevB.64.115411) (2001).
23. Palacios, J. J., Pérez-Jiménez, A. J., Louis, E., SanFabián, E. & Vergés, J. A. First-principles approach to electrical transport in atomic-scale nanostructures. *Phys. Rev. B* **66**, 035322, DOI: [10.1103/PhysRevB.66.035322](https://doi.org/10.1103/PhysRevB.66.035322) (2002).

24. Louis, E., Vergés, J. A., Palacios, J. J., Pérez-Jiménez, A. J. & SanFabián, E. Implementing the keldysh formalism into ab initio methods for the calculation of quantum transport: Application to metallic nanocontacts. *Phys. Rev. B* **67**, 155321, DOI: [10.1103/PhysRevB.67.155321](https://doi.org/10.1103/PhysRevB.67.155321) (2003).
25. Palacios, J. J. *et al.* Computer code ANT.Gaussian, with SOC corrections. Available from <https://github.com/juanjosepalacios/ANT.Gaussian>.
26. Zöllner, M. S., Saghatchi, A., Mujica, V. & Herrmann, C. Influence of electronic structure modeling and junction structure on first-principles chiral induced spin selectivity. *J. Chem. Theory Comput.* **16**, 7357–7371, DOI: [10.1021/acs.jctc.0c00621](https://doi.org/10.1021/acs.jctc.0c00621) (2020).
27. Yang, X., van der Wal, C. H. & van Wees, B. J. Spin-dependent electron transmission model for chiral molecules in mesoscopic devices. *Phys. Rev. B* **99**, 024418 (2019).
28. Guo, A.-M. *et al.* Contact effects in spin transport along double-helical molecules. *Phys. Rev. B* **89**, 205434, DOI: [10.1103/PhysRevB.89.205434](https://doi.org/10.1103/PhysRevB.89.205434) (2014).